EUMETSAT ECMWF

EUMETSAT Contract Report

EUMETSAT EUM/CO/22/4600002673/SDM

Contract Report to EUMETSAT

Task 1.1 Evaluation of initial future EPS-Sterna constellations with 50 and 183 GHz

Final report for Task 1.1, EUMETSAT contract no. EUM/CO/22/4600002673/SDM

Authors: Katie Lean, Niels Bormann and Sean Healy

September 2023

Series: EUMETSAT/ECMWF Contract Report Series

A full list of ECMWF Publications can be found on our web site under:
http://www.ecmwf.int/en/publications/

Contact: library@ecmwf.int

European Centre for Medium Range Weather Forecasts, Shinfield Park, Reading, RG2 9AX, UK

Contents

Abstract

Observations from space-borne microwave (MW) sounding instruments currently provide a very important contribution to accurate Numerical Weather Prediction (NWP) forecasts. Complementing a continuing backbone of high-performance satellite platforms, small satellites are expected to become a significant component of the future observing system. The future EPS-Sterna constellation will consist of small satellites carrying MW sounding instruments. The EPS-Sterna instrument comprises well-established frequencies in the 50 and 183 GHz bands (plus complementary window channels) and a new set of channels around 325 GHz not seen on a space-borne platform before.

In this first phase of the project, we simulate the potential benefit of initial options for the EPS-Sterna constellations with focus on the 50 and 183 GHz frequencies. The different scenarios are assessed using the Ensemble of Data Assimilations (EDA) method where changes to the EDA spread (indicating changes in forecast uncertainties) inform the relative benefits of different constellations. A framework to flexibly simulate and assimilate MW sounders on small satellites within the all-sky framework has already been developed at ECMWF. We build on this existing work here and present a summary of the different steps and modifications required for the EPS-Sterna instrument. The simulated EPS-Sterna data and accompanying observation errors are added to a baseline of existing observations. Four EPS-Sterna scenarios are considered: a configuration proposed for nominal operational use consisting of six satellites in three orbital planes, two degraded options which add three satellites in three orbital planes and four satellites in two orbital planes respectively, and an enhanced option of eight satellites in four orbital planes. In addition to testing the different constellations, several EDA experiments are also run which change either the number of existing MW observations or deny entire Metop platforms relative to the same reference baseline.

The EDA analysis reveals that all four EPS-Sterna scenarios produce a significant positive impact for a range of atmospheric variables, including temperature, geopotential, wind and relative humidity. The impact increases with the number of satellites, and the six-satellite scenario gives just under twice the impact of the three-satellite scenario. Impacts are largest in the southern hemisphere and smallest in the tropics, in line with the trend for changes to real MW sounding observation numbers. Comparison to EDA impacts from changes to real data reveals that EPS-Sterna is able to achieve additional benefit that compares well to the magnitude of impact seen with similar numbers of existing MW sounders. Based upon EDA spread reductions across a range of variables, we would expect the six-satellite EPS-Sterna constellation to have an impact of between one and two full Metop platforms and thus provide significant additional benefits for global NWP, provided the EPS-Sterna data quality is acceptable. However, it is noted that this constellation of small satellites cannot replace the full, wide-reaching impacts of a high-performance, multi-sensor platform. Further sensitivity EDA experiments explore the impact of instrument noise performance by separately inflating or reducing the values. A degradation of 30% in instrument noise values for the six-satellite scenario equates to the loss of between one and two satellites in the constellation in the extra-tropics. A reduction in noise of around 60% in only the temperature sounding channels resulted in further spread reduction exceeding the benefit from adding two more small satellites in the extra-tropics, emphasising the importance of pursuing good noise performance especially for temperature sounding channels.

We also use the EDA method to demonstrate potential large positive impact from combining the six-satellite EPS-Sterna constellation with a future Doppler Wind Lidar (DWL) based on EPS-Aeolus (assessed in a separate study), the follow-on mission to Aeolus. The resulting benefit seen globally and across the pressure levels from assimilating the two missions together arises from good complementarity of the independent mission contributions to the EDA spread reduction and the largely additive nature of the separate impacts. For example, large positive impacts on tropical wind in the combined experiment is attributed mainly to the DWL while impacts on geopotential height in the extra-tropics have a higher contribution from EPS-Sterna.

1 Introduction

Microwave (MW) sounding instruments on satellites form a vital component of the observing system used in Numerical Weather Prediction (NWP) (Bormann et al., 2019). There is clear evidence from analysis of existing instruments for significant advantages from additional MW data (Duncan et al., 2021) beyond the CGMS 3-orbit baseline (EUMETSAT, 2019). At present, we are in a fortunate era of receiving MW temperature and humidity sounding data from several high-performance instruments on large satellite platforms. Furthermore, the addition of MW data to this already mature system continues to be beneficial (Duncan and Bormann, 2020). However, some of the existing satellites are already functioning well beyond their expected design-lifetime or will be decommissioned and with few replacements confirmed, the constellation of these large platforms is expected to decrease.

Constellations of small satellites are increasingly being considered as a future component of the observing system which would be complementary to a reduced number of high-performance, large platforms. Improvements in the ability to miniaturise technology have allowed the possibility of MW sounding instruments on small satellites that still maintain a level of performance suitable for use in NWP. While there are some compromises, such as the difficulty in accommodating lower frequencies (less than 50 GHz) or potentially poorer noise performance, the advent of these smaller platforms provides a cost-effective way to improve the temporal sampling. In particular, enhanced temporal sampling can allow better observation of faster evolving cloud, humidity and precipitation features as well as reducing the random component of noise through more repetitive measurement.

A recent ESA-funded study considered the design of constellations of small satellites carrying MW sounding instruments for global NWP. It showed that positive impact continued to increase from adding more MW sounding observations, though for large constellations (20 small satellites) the gain in benefit appeared to slow (Lean et al., 2022b). The study further showed that significant benefit can be achieved with a constellation of eight small satellites added to a baseline with a reduced number of existing larger platforms (reflecting the potential future decline in these platforms). Results also highlighted the extra positive impact from temperature sounding observations around 50 GHz when compared to using humidity sounding capabilities only, suggesting that they would be a worthwhile addition to small satellite platforms where they can be sensibly accommodated.

The importance of continuing and even expanding the essential role of MW sounding data is recognised in the EUMETSAT proposal of the EPS-Sterna constellation which will consist of polar-orbiting small satellite platforms that each carry a MW sounding instrument (e.g. https://www.eumetsat.int/eumetsat-invests-development-new-weather-and-climate-satellite-systems). The payload proposed for the EPS-Sterna constellation is the same as the Arctic Weather Satellite (AWS), to be launched by ESA in 2024, with the design of the constellation aspects still in review. The instrument characteristics and channel selection for the instrument on AWS and EPS-Sterna have been derived from those of the Microwave Sounder (MWS) for the EUMETSAT Polar System – Second Generation (EPS-SG) (MWS Science Advisory Group, 2019; EUMETSAT, 2019). The EPS-Sterna instrument is a 19 channel cross-track scanning radiometer that includes sounding channels around 50 and 183 GHz which sample oxygen and water vapour absorption bands respectively, together with selected window channels at 89 and 165.5 GHz (e.g. https://www.esa.int/aws). These frequencies are routinely used in the all-sky assimilation framework at ECMWF from a range of MW instruments (Geer et al., 2014; Duncan et al., 2022). Additionally, the EPS-Sterna instrument will have a novel suite of four channels centred around 325 GHz which also exploit a water vapour absorption band. These channels have not been flown before on a space-borne instrument but are expected to provide additional information, for example, due to scattering from smaller ice particles than at 183 GHz

(Eriksson et al., 2020). In this EUMETSAT-funded study, we investigate potential configurations for the EPS-Sterna constellation and estimate the added benefit of the new 325 GHz channels. Furthermore, we explore the sensitivity to the instrument noise performance by additionally testing one scenario with inflated and reduce noise performance.

Previous work has addressed broad questions regarding constellation design of small satellites carrying MW instruments (Lean et al., 2022b) and we use this experience in order to now focus on probing design aspects of the potential future EPS-Sterna constellation. Complementary to earlier work, the project examines constellations with fewer satellites, filling a gap in satellite numbers that was not explored previously (where the minimum constellation started at eight satellites). Particular aspects to be considered during the project are:

- What is the relative benefit of each constellation ranging from degraded to more ambitious options?
- How do the estimated benefits of EPS-Sterna compare to impacts of real data?
- How much additional benefit do the channels at 325 GHz provide?

As in earlier work, the Ensemble of Data Assimilations (EDA) method is used to assess the relative benefit to NWP of the different EPS-Sterna scenarios and additional impact from the new 325 GHz channel set. The EDA method uses a Monte-Carlo approach to estimate the forecast uncertainty in data assimilation. Impacts from new observations are evaluated by comparing EDA simulations with and without the added observations, and the EDA spread is taken as the key measure of changes in the forecast uncertainty. The method has in the past also been used to assess the expected impact from Aeolus observations (Tan et al., 2007) and from increases in the number of radio occultation measurements (Harnisch et al., 2013). The present study builds heavily on the framework developed to use the EDA technique to assess small satellite constellations with MW sounding instruments as part of the earlier ESA study (Lean et al., 2022b). Furthermore, we explore the sensitivity to the instrument noise performance by additionally testing one scenario each with inflated and reduced instrument noise, respectively. Bell et al. (2010) have demonstrated by conducting OSE experiments with AMSU observations that significant degradation in forecast skill can be seen with increases in NEDT.

In addition to the evaluation of EPS-Sterna, a parallel EUMETSAT-funded study at ECMWF has also used the EDA method to consider the benefits of EPS-Aeolus, a Doppler Wind Lidar (DWL) follow-on mission to Aeolus ("Aeolus2"). The analysis of Aeolus2 is presented in detail in a separate report (Healy et al., 2023). The proposed EPS-Sterna and EPS-Aeolus missions are expected to significantly overlap in lifespan so here we also consider the complementarity of EPS-Sterna and EPS-Aeolus and the additional impact from assimilating both missions simultaneously. Note that the analysis of combining the missions presented here is replicated in Healy et al. (2023) for convenient reference.

In this first report of the EPS-Sterna project, we present outcomes from task 1.1 which concerns the evaluation of an initial set of constellations with frequencies at 50 and 183 GHz (plus window channels). Developing the strategy for assimilating the 325 GHz is still ongoing and will be included in further scenarios investigated in a subsequent project task. In this way, the results from the first constellations evaluated here provide a comparison to better quantify the impact of the additional 325 GHz channels but also help to inform what further constellation configurations would be desirable to test. Section 2 outlines key aspects of the EDA methodology and the experimental set up. Initial scenarios chosen to evaluate the reduced channel set and additional experiments where changes have been made to existing observations are discussed in section 3. Instrument noise performance details are also provided here for use in sensitivity experiments. Section 4 reviews the framework already developed (Lean et al., 2022a),

and any modifications, which allows the flexible simulation and assimilation of EPS-Sterna MW data. Results of the EDA experiments are presented in section 5, including the combined experiment with an EPS-Aeolus-like mission, and conclusions from this first part of the study discussed in section 6.

2 Use of the Ensemble of Data Assimilations to assess observation impact

In the following, we outline key aspects of the EDA methodology used to assess the impact of future observations and present the experimental set up for evaluating the EPS-Sterna constellations. The EDA concept was explored in detail in the earlier ESA study allowing us to use this foundation of existing knowledge here. Therefore we present only a summary of the technique. Further details can be found in Lean et al. (2021a,b). Note that technical explanation of the methodology and a review of differences between the EDA and Observing System Simulation Experiments (OSSEs) have been largely reproduced from the final ESA report (Lean et al., 2022b).

2.1 Methodology of the EDA

The EDA is used at ECMWF and elsewhere to represent random uncertainties in analyses and short-range forecasts of large NWP systems (Isaksen et al., 2010). It uses a Monte-Carlo approach to estimate the statistical characteristics of errors in analyses and short-range forecasts from the uncertainties in input parameters and the forecast model. This is done by running a finite number of independent cycling assimilation systems, in which observations and the forecast model are perturbed to generate different inputs for each member. The following aspects are perturbed in the EDA:

- Observations: These are perturbed according to the observation error covariances assigned in the assimilation system, assuming a Gaussian distribution with zero mean (Isaksen et al., 2010).
- Forecast model: Model error is represented by stochastic perturbations of the model physics (carried out using the Stochastically Perturbed Parametrised Tendency (SPPT) scheme, (Palmer et al., 2009)).
- Sea surface temperature (SSTs): These are perturbed according to climatological error structures.

Mathematically, the errors from the perturbed realisation of 4D-Var evolve with the same equations as the errors of the unperturbed version (see Lean et al. (2021a) which provides a summary of the mathematical details). A crucial measure of the EDA is the ensemble spread, i.e. the standard deviation of the ensemble members around the ensemble mean as given in the following equation:

$$s = \sqrt{\frac{1}{D}\sum_{d=1}^{D}\left[\frac{1}{N-1}\sum_{n=1}^{N}(\mathbf{x_n}-\bar{\mathbf{x}})^2\right]_d} \tag{1}$$

Where s is the spread, D is the required time period e.g. the number of model cycles, N is the size of the ensemble (10 members for this study), $\mathbf{x_n}$ is the model state from a single ensemble member and $\bar{\mathbf{x}}$ is the ensemble mean. If the characteristics of the perturbations in the ensemble members correctly represent the true errors, the spread of the ensemble will reflect the errors in analyses and forecasts.

At ECMWF, the EDA method has been operationally used since June 2010 (Isaksen et al., 2010; Bonavita et al., 2011) to fulfil two key requirements:

- Specification of background error statistics: The EDA is used to provide climatological as well as flow-dependent estimates of the statistical properties of the errors in the short-range forecasts (background) used in the high-resolution deterministic assimilation system. To capture flow-dependent aspects, an EDA is run alongside the high-resolution deterministic forecast system.
- Initialisation of the ensemble prediction system: Perturbations from the EDA are used together with Singular-Vector methods to initialise ECMWF's ensemble prediction system which provides probabilistic medium-range forecasts.

Operationally, 50 EDA members are currently used at ECMWF. The number of members used in the ensemble is a trade-off between computational affordability and reducing sampling noise in the background error estimates. For research-purposes EDAs with 10 members have been found to provide adequate estimates, at least for background error variances on larger scales.

2.2 Application of the EDA to simulate impact of future observations

By evaluating changes in EDA spread, the EDA approach provides estimates of the impact of potential future observations on analysis and short-range forecast error statistics. The spread will be affected by the addition or modification of simulated (or real) observations to the EDA. Positive impact is associated with reductions in EDA spread, i.e. indicating a reduction in the uncertainties and therefore improved analysis/forecast error statistics. To assess the impact of potential EPS-Sterna constellations, we choose a baseline observing system of real observations (detailed in section 3) and add simulated MW observations based on different proposed scenarios. These simulated data can be produced, for example, from high resolution NWP analyses. An accurate estimate of the observation errors associated with the simulated data is also critical as they form the basis of realistic perturbations applied to the observations within the EDA.

The approach has been applied to other observation types having been first developed to investigate the expected impact of wind profile observations from Aeolus (Tan et al., 2007). It was later used to estimate the impact of increasing the number of Global Navigation Satellite System (GNSS) Radio Occultation (RO) observations with a view to provide guidance for future constellation design aspirations (Harnisch et al., 2013). Subsequently, the advent of new satellites has allowed verification of this assessment by testing with real data. Lonitz et al. (2021) showed that the relative benefits predicted while using simulated data are in line with the impacts obtained from adding real data. Most recently, the EDA technique has been applied to investigating broad questions around the design of a potential future constellation of small satellites carrying MW instruments (Lean et al., 2022b), which forms the basis of the present work.

The EDA method has similar aims as the more traditional OSSEs (Arnold and Dey, 1986; Masutani et al., 2010). In these, simulated observations are generated from a "truth" - the "nature run" - and subsequently assimilated in an alternative forecast system (e.g. Masutani et al. (2007)). To achieve this, all the observations from both the existing and proposed new sources need be simulated, including their full error characteristics. This means that OSSEs can be problematic if errors are not adequately modelled for all observations. OSSEs are also computationally expensive, as long periods are required to establish statistically robust results. Meanwhile Tan et al. (2007), Harnisch et al. (2013) and Lean et al. (2021a) consistently show that relatively short EDA experimentation periods, of the order of one month, are sufficient which was motivated by relatively stable characteristics of the EDA spread. OSSEs and the EDA method are seen as complementary (Harnisch et al., 2013).

The EDA method can also be thought of as a 4D-Var theoretical error covariance/-information content

study. Computing 4D covariance matrices directly is not practical due to the very large matrix dimensions required. However, the spread in the ensemble members provides an estimate of analysis/forecast error statistics of the 4D atmospheric state which includes the impact of a complex observing system and forecast model. Therefore, one of the key differences in the metrics available from OSSEs and the EDA method is that the former evaluates one specific realisation of forecast error, evaluated against the "truth" from the nature run, while the latter aims to evaluate directly the statistical characteristics of the forecast error.

The EDA method is of course also not free from limitations either. Firstly, the method assumes that the perturbations applied in the EDA reflect the true error characteristics, but in practice these are both subject to their own uncertainties. Secondly, the EDA is a Monte Carlo method so the true values are only found in the limit of an infinite ensemble. This results in sampling errors from a finite ensemble size (Bonavita et al., 2011) and systematic errors can arise from incorrectly estimated error covariances (e.g. Cardinali et al. (2014)). By averaging over larger areas, such as hemispheric scales, small scale sampling errors can be reduced while keeping the large-scale changes in the EDA spread. Harnisch et al. (2013) also note that systematic short-comings are likely to be similar across a set of experiments run with consistent settings and therefore the magnitudes of relative changes are unaffected. Finally, for both the EDA and OSSE methods, both can only assess the impact reflecting the current treatment of the observations. Neither system can account for the impact of unknown future developments that could potentially change the priorities in MW sounder design, or similarly for investigating impacts of other observation types.

To further confidence in the EDA method, links have been established between impact as measured by changes in EDA spread and more traditional measures of forecast impact given by Observing System Experiments (OSEs) (Lonitz et al., 2021; Lean et al., 2021b, 2022b). The calculation of forecast error focused on using radiosondes as a reference measurement against which the short-range forecast could be compared. Analysis was carried out using sets of experiments where changes were made to existing observations – varying the number of GNSS-RO and MW sounding observations in separate studies. The results were consistent and demonstrated clear evidence of a relationship that relative changes in EDA spread compare well with results from OSEs. However, while this confirmed that the EDA is a useful indicator of changes in short-range forecast skill, a simple one-to-one relationship is not applicable. The difficulty in deriving a quantitative link highlighted the under-dispersive nature of the EDA (i.e. that the forecast impact measured by the radiosondes is larger than estimated by the EDA spread reduction) which is a known characteristic of the EDA (Bonavita et al., 2012).

2.3 EDA experimental set up

All the EDA experiments run in this study and the parallel EPS-Aeolus study employ a standard experiment configuration used routinely at ECMWF for operational development testing and previously used in testing future observing systems. It comprises one control member and 10 perturbed members and employs a $T_{Co}399$ (25km) resolution grid with 137 vertical levels and three inner loops at a resolution of $T_L95/T_L159/T_L255$ (210/125/80 km). Experiments are run over a four-week period spanning 1 – 28 July 2019. This time period was chosen as key MW instruments as well as other significant components of the observing system are stable and performing well. Additionally, good quality re-processed Aeolus data are available at this time which permits use of a common test period to conduct the parallel future DWL study and allow combined experiments with the EPS-Sterna constellations. Previous experience has shown that, after discarding the first week of statistics while the EDA develops representative levels of spread, the remaining three weeks are sufficient to provide robust estimates of EDA spread changes

(Lean et al., 2021a). EDA spread changes are calculated at a resolution of T_L255 (80 km, the highest resolution inner loop of the experiment) and at T+12 hours, as short lead times are expected to exhibit the most robust signals. As the forecast length increases, model uncertainties increase, reducing the clarity of signals introduced by observation changes (Harnisch et al., 2013).

3 Potential EPS-Sterna constellations (50 and 183 GHz)

In this first task of the project, the focus has been on assessing an initial set of constellations that consider the well-established 50 and 183 GHz channels (plus complementary window channels). Results from these early scenarios will inform which constellations to test with the additional 325 GHz. The set of scenarios is chosen to probe how the impact varies with the number of available satellites and orbital planes, with a maximum number of four orbital planes covered. For each scenario, the EPS-Sterna observations are simulated and added to a Baseline observing system of real observations for assimilation in an EDA experiment. This Baseline utilizes the full observing system in operational use in July 2019 but with a reduced number of MW sounding instruments to reflect a future where the number of current larger platforms will be depleted. The real MW sounders used in this Baseline are constructed from two pairs of Advanced Microwave Sounding Unit – A/Microwave Humidity Sounder (AMSU-A/MHS) on Metop-B/C, two Advanced Technology Microwave Sounder (ATMS) instruments on SNPP/NOAA-20, AMSU-A on NOAA-15 and 183 GHz channels on the Special Sensor Microwave Imager/Sounder (SSMIS) on the F-17 platform. These reflect the early morning, mid-morning and afternoon orbital planes defined as high priority to maintain (Coordination Group for Meteorological Satellites, 2022). Further to these polar-orbiting platforms, the Global Precipitation Measurement (GPM) Microwave Imager (GMI) is included in the Baseline which carries 183 GHz channels and flies in a mid-inclination orbit of 65°, observing the tropics and mid-latitudes. Note that Aeolus observations are not assimilated in the Baseline; the same Baseline is used in the experimentation for the future Doppler Wind Lidar.

To provide context to the results from adding the simulated data, further EDA experiments have been run in which the existing observing system used has been changed compared to the Baseline (table 1). Adding or denying MW sounding observations allows points of reference to gauge the impact of the simulated data. It also provides a means to verify whether the results for the simulated future observations are consistent with findings with real data (consistent with previous findings (Lean et al., 2022b)). Whole multi-sensor satellite platforms (Metop-C alone or both Metop-B and -C) have also been denied in further experiments i.e. not just removing MW sounding data. This is to provide links in NWP impact to socio-economic studies conducted previously, e.g. for the Metop platforms (Hallegatte et al., 2014). In the EDA experiments here, the following types of data are assimilated from Metop-B/-C: hyperspectral infrared sounding (Infrared Atmospheric Sounding Interferometer (IASI)), GNSS-RO (GNSS Receiver for Atmospheric Sounding (GRAS)), surface winds (Advanced Scatterometer (ASCAT)) and tropospheric winds (Atmospheric Motion Vectors (AMVs) derived from the Advanced Very High Resolution Radiometer / 3 (AVHRR/3)). Note that additional Metop products such as ozone and nitrogen dioxide products from Global Ozone Monitoring Experiment – 2 (GOME-2) are not included in the EDA here but are used by ECMWF within atmospheric composition services.

Initially, four potential future EPS-Sterna constellations carrying MW instruments are considered (table 2). These have been devised by EUMETSAT and feature the scenario proposed as the nominally operational configuration consisting of three orbital planes with two satellites in each plane (“OP3-6SAT”). Two smaller constellations with smaller numbers of satellites represent degradation from this preferred six-satellite scenario either with a reduced number of orbital planes (“OP2-4SAT”) or fewer satellites in each plane (“OP3-3SAT”). A further scenario adds two satellites to the nominally operational configura-

Table 1: Combinations of existing MW sounders on sun synchronous platforms used in EDA experiments containing only real data evaluated using the EDA method. Note that in all cases apart from R1, GMI is also assimilated. R1-R4 concern adding/denying polar orbiting MW sounding instruments where R2 is the reference baseline to which all simulated EPS-Sterna data are added. R5 and R6 involve the denial of all assimilated instruments on the satellite platforms. LECT = Local Equator Crossing Time.

Index	Experiment name	MW sounder platform	LECT of MW sounders
R1	No MW sounding	None	-
R2	Baseline	Metop-B/C AMSU-A/MHS, SNPP ATMS, NOAA-20 ATMS, NOAA-15 AMSU-A, F-17 SSMIS	2x09:30, 2x01:30, 1x07:00, 1x06:30
R3	3 MW Sounders	Metop-B AMSU-A/MHS, NOAA-20 ATMS, NOAA-15 AMSU-A, F-17 SSMIS	1x09:30, 1x01:30, 1x06:30, 1x07:00
R4	7 MW Sounders	R2 + NOAA-18/-19 AMSU-A/MHS	2x09:30, 2x01:30, 1x07:00, 1x06:30, 1x08:30, 1x04:30
R5	Metop-C denial	R2 with denial of Metop-C platform	1x09:30, 2x01:30, 1x06:30, 1x07:00
R6	Metop-B/-C denial	R2 with denial of Metop-B/-C platforms	2x01:30, 1x06:30, 1x07:00

tion to create an "enhanced" option of four orbital planes with two satellites in each plane ("OP4-8SAT"). Figure 1 illustrates a typical example of the coverage of the individual subsatellite points for each of the constellations. In each case, the LECTs and phasing of multiple satellites within each orbital plane have been optimised while accounting for the existing MW sounders in the Baseline system. The satellite positioning in the nominally operational and degraded options have been tuned by EUMETSAT (pers. comm. J. Ackermann) to minimise the time to achieve global coverage while also distributing the satellites to minimise overlap of the swaths. The latter of these criteria helps to reduce large geographical gaps in coverage over shorter periods of time and also mitigates against losing a higher proportion of data that sample the same area during spatial thinning processes (discussed later in section 4.2). In the eight-satellite "enhanced" scenario the fourth plane is added to OP3-6SAT without any adjustment to the sampling of satellites already optimised for three planes.

The current study uses the EPS-Sterna instrument specifications (e.g. https://www.esa.int/aws, Lagaune et al. (2021)), with the exception of the instrument noise for which realistic estimates based on pre-launch testing of AWS are used. The instrument is a cross-scanning radiometer comprising 115 fields of view (FOV) with a maximum scanning angle from nadir of 54.4293° and is expected to be flown at an altitude of 600km. The instrument mass is expected to be around 120kg which allows a good compromise between drawbacks from miniaturisation, such as the loss of the low frequencies, while retaining performance comparable to the existing MW instruments for common frequencies. A summary of the EPS-Sterna instrument frequencies and their key characteristics, including the noise performance (latest estimates after pre-launch instrument testing at the time of EDA experimentation, pers. comm., S. Di Michelle) is given in table 3. Note that the table provides values of the sample (or raw) NEDT which accounts for the integration time for one FOV on the instrument. This differs from the NEDT definition used in the EPS-Sterna instrument user requirements which instead gives values based

Table 2: Potential future EPS-Sterna constellations comprising small satellites in sun synchronous orbits carrying MW sounders evaluated using the EDA method. Constellations include a six-satellite scenario favoured for future operational implementation and further scenarios representing degradations or enhancement to this nominally operational configuration. Each of the constellations are added to the reference Baseline (R2, table 1) and are run with temperature and humidity sounding channels only at 50 and 183 GHz respectively (plus complementary window channels). LECT = Local Equator Crossing Time.

Scenario no.	Experiment name	LECT	No. of planes	No. of satellites per plane	Total no. of satellites
1	OP3-6SAT "nominally operational"	2x03:30, 2x07:30, 2x11:30	3	2	6
2	OP3-3SAT "degraded 1"	1x03:30, 1x07:30, 1x11:30	3	1	3
3	OP2-4SAT "degraded 2"	2x03:30, 2x11:30	2	2	4
4	OP4-8SAT "enhanced"	2x03:30, 2x05:30, 2x07:30, 2x11:30	4	2	8

on the time for the antenna to cover an angle equal to the 3dB beam width (e.g., Atkinson (2015)), which are typically smaller.

To test the sensitivity to the noise performance of the instrument two further EDA experiment using only the OP3-6SAT scenario are run where the NEDT values of all channels are inflated by 30% and secondly the noise on temperature sounding channels only is reduced by around 55-60% (table 4). By inflating values by 30% some of the temperature sounding channels have NEDT higher than the instrument specifications. Stringent requirements are placed on the noise performance of MW instruments, particularly for the temperature sounding channels in the 50 GHz band, in order to significantly benefit NWP where tropospheric temperature errors are already small (Bell et al., 2008). For the set of reduced NEDT values, only the temperature sounding channels in the 50 GHz band have been changed as the benefit from these channels is expected to be most sensitive to the noise performance. The chosen values are significantly lower than current estimates of realistic sample NEDT. They are inadvertently based on pre-launch measurements of the 3dB NEDT, but without the 1.73 scaling factor to obtain the sample NEDT. It is hence likely that such performance is not achievable from a small satellite. The results are nevertheless included here as a hypothetical scenario, to illustrate the potential benefit of better noise performance irrespective of whether engineering solutions can be found to achieve such performance in the future, either on small or larger platforms.

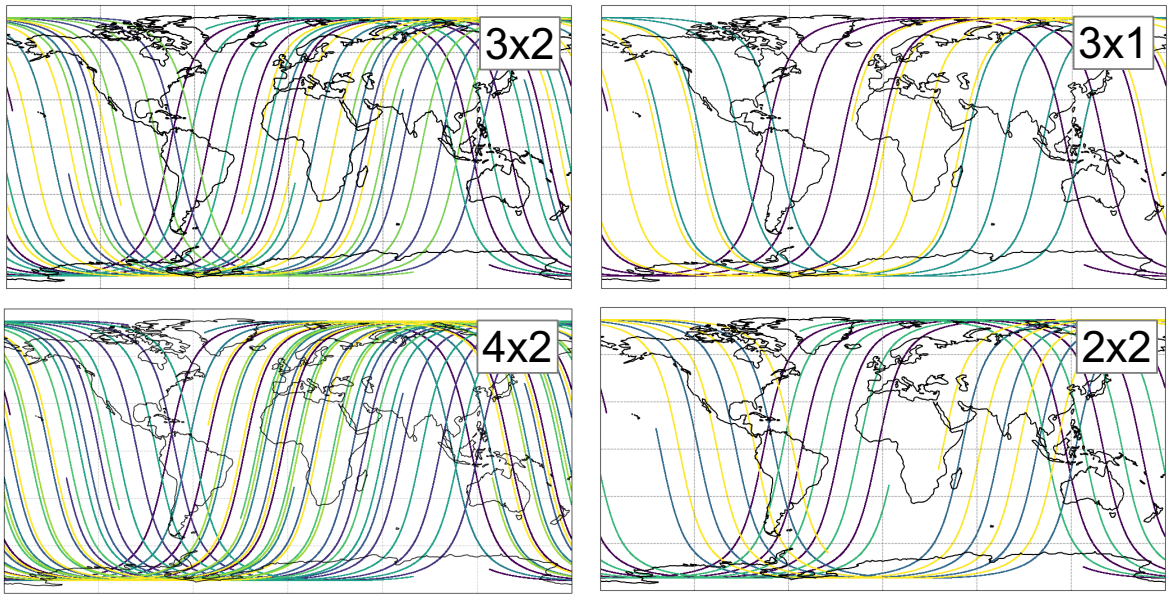

Figure 1: Maps showing an example of the typical subsatellite point coverage for each of the satellites in the four initial EPS-Sterna constellations (clockwise from top left: OP3-6SAT (nominally operational configuration), OP3-3SAT, OP2-4SAT and OP4-8SAT scenarios). Data are for a six-hour period, 03:00 – 09:00 2 July 2019. Colours are only used to differentiate the individual satellites within each constellation.

4 Framework for simulating and assimilating EPS-Sterna MW data

In the present study we adapt the framework previously developed in an ESA-study used to assess the potential for a range of future constellations with MW sounding observations. While a brief summary of the steps are presented in the following section, full details of the system design can be found in (Lean et al., 2022a). In this first task, the 325 GHz channels are not considered and therefore at this stage, it is possible to exploit the existing infrastructure already in place for the well-established frequencies around 50 and 183 GHz. Methods to treat the new high frequency channels will be developed and presented in a subsequent report. Note that EPS-Sterna instrument channel 3 (53.246 GHz) has also not been assimilated before at ECMWF. However, this new frequency lies between the frequencies of two well-established channels in a well understood part of the frequency spectrum. Therefore, we can have confidence in the quality of simulated observations without need for special treatment and can draw on the examples of the neighbouring channels to apply very similar approaches during assimilation.

4.1 Simulating EPS-Sterna MW brightness temperatures

The simulation of the data uses a tailored version of the Integrated Forecast System (IFS) to take high resolution NWP model fields, interpolate to the observation locations and convert them to brightness temperatures (BTs) with application of a radiative transfer model. For the EPS-Sterna constellations, simulated BTs are produced using a version of the IFS based on cycle 47R3.4 (operational at that time) but with adaptations to include the latest package of MW improvements that will be used at the next IFS cycle upgrade. High resolution (($T_{Co}1279$, ∼9km, 137 vertical levels) ECMWF analyses are used as a

Table 3: Specifications for channels used in the small satellite simulation for all scenarios in table 2. Note that the values of instrument noise correspond to the sample NEDT which are scaled values of the 3dB Field of View (FOV) NEDT, accounting for the sampling interval of the instrument rather than using the time for the antenna to cover an angle equal to the 3dB beam width.

Centre frequency (GHz)	MW instrument channel	AMSU-A/MHS channel	Bandwidth (MHz)	Footprint size at nadir (km)	Sample NEDT (K)
50.3	1	AMSU-A 3	180	40	0.987
52.8	2	AMSU-A 4	400	40	0.641
53.246	3	-	300	40	0.641
53.596	4	AMSU-A 5	400	40	0.658
54.4	5	AMSU-A 6	400	40	0.606
54.94	6	AMSU-A 7	400	40	0.606
55.5	7	AMSU-A 8	330	40	0.641
57.290344	8	AMSU-A 9	330	40	0.658
89	9	AMSU-A 15/MHS 1	4000	20	0.269
165.5	10	MHS 2 (157GHz)	2800	10	0.53
176.311	11	MHS 5	2000	10	0.53
178.811	12	-	2000	10	0.53
180.311	13	MHS 4	1000	10	0.74
181.511	14	-	1000	10	0.74
182.311	15	MHS 3	500	10	1.04
325.15±1.2	16	-	800	10	1.42
325.15±2.4	17	-	1200	10	1.16
325.15±4.1	18	-	1800	10	0.95
325.15±6.6	19	-	2800	10	0.76

proxy for the truth. Spatial/temporal sampling information to interpolate the model fields to observation locations is given by orbital parameter files provided by EUMETSAT. The radiative transfer modelling is performed using RTTOV-SCATT[1] (version 13) which accounts for scattering from hydrometeors at MW frequencies and therefore allows use of the MW data in the all-sky framework (Saunders et al., 2020; Geer et al., 2021). RTTOV-SCATT coefficient files were provided by the NWP SAF (https://nwp-saf.eumetsat.int/site/software/rttov/download/coefficients/coefficient-download/) and they are used throughout this study.

The process is very similar for simulating the EPS-Sterna MW data as for generating model equivalent BTs for real data however there is one exception related to emissivity calculation over land, snow and sea-ice surfaces. For real MW data over these surfaces, emissivity used for deriving the equivalent BTs of surface sensitive sounding channels is obtained through a dynamic emissivity retrieval from window channels (Karbou et al., 2006). During the simulation process, this is replaced by use of an emissivity atlas over land and a relatively crude approximation over snow and sea-ice surfaces, whereas during the subsequent assimilation the dynamic retrieval approach is used. As a result of using these simplistic values as initial input for the emissivity, the simulation of the impact of EPS-Sterna is likely

[1]RTTOV = Radiative Transfer for TOVS, TOVS = TIROS Operational Vertical Sounder, TIROS = Television Infrared Observation Satellite

Table 4: NEDT values for sensitivity experiments which compare the original NEDT used in all four EPS-Sterna scenarios (reproduced from table 3) alongside all values inflated by 30%, values in the 50 GHz band reduced by 55-60% and, for reference only, maximum values given by the instrument requirements. Values for the 325 GHz are not included here as they are not assimilated in these EDA experiments.

Centre frequency (GHz)	MW instrument channel	Original sample NEDT (K)	Inflated NEDT (K)	Reduced NEDT (K)	NEDT requirements (K)
50.3	1	0.99	1.28	0.37	1.04
52.8	2	0.64	0.83	0.25	0.69
53.246	3	0.64	0.83	0.28	0.69
53.596	4	0.66	0.86	0.25	0.69
54.4	5	0.61	0.79	0.25	0.69
54.94	6	0.61	0.79	0.24	0.69
55.5	7	0.64	0.83	0.28	0.87
57.290344	8	0.66	0.86	0.31	1.04
89	9	0.269	0.35	0.27	0.42
165.5	10	0.53	0.69	0.53	0.60
176.311	11	0.53	0.69	0.53	0.70
178.811	12	0.53	0.69	0.53	0.70
180.311	13	0.74	0.96	0.74	1.00
181.511	14	0.74	0.96	0.74	1.00
182.311	15	1.04	1.35	1.04	1.30

to be optimistic over snow and sea-ice surfaces. For results in the northern hemisphere, this is mitigated by choosing a northern hemisphere summer period for the experimentation performed in this study. Further details can be found in Lean et al. (2022a). Note that improved forward-modelling for passive MW observations affected by surface snow and sea-ice is an area of active research, and simulation and assimilation of EPS-Sterna and AWS data will benefit from any advances in this area.

4.2 Sampling and thinning

For global NWP, the noise performance of the assimilated observations is critical for the temperature-sounding channels, for which errors in NWP are small (within the order of tenths of a kelvin (Bell et al., 2008)). When the noise of individual observations is comparatively high, averaging (or "super-obbing") is often applied, in order to reduce the effective noise in the assimilated data. This is for instance done for ATMS, for which a 3x3 averaging technique is applied, taking advantage of the spatial oversampling of the observations (Bormann et al., 2013). For humidity-sounding channels, such super-obbing can also reduce spatial representativeness errors, that is mismatches in the scales represented in the observations and the model fields. Analysis of different choices for the number of FOVs to average found that 3x3 was also an appropriate choice for an EPS-Sterna-like instrument, where there is spatial oversampling. The choice of 3x3 averaging brings the effective noise characteristics of the temperature-channels down to levels more comparable to that of existing MW observation use (Lean et al., 2022b). Therefore, the same strategy is used here. In practice though, for simplicity, we chose not to perform explicit averaging

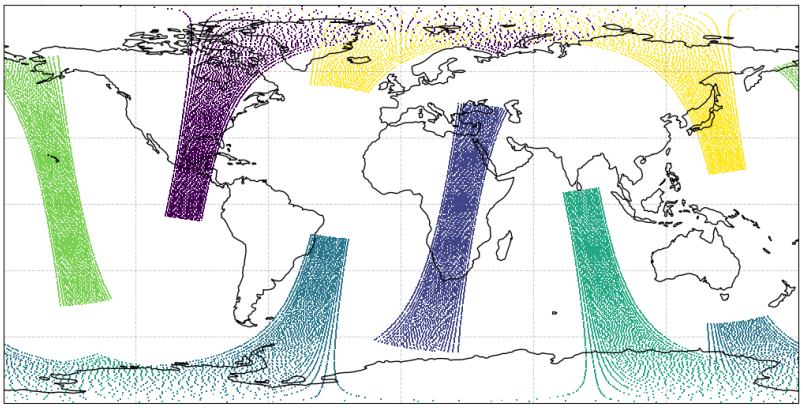

Figure 2: Map showing an example of the typical coverage of simulated MW observation locations for the nominally operational, OP3-6SAT constellation after both sampling to mimic 3x3 averaging and thinning all satellites together. Data are for a 30-minute time slot (09:30 to 10.00) on 1 July 2019. Colours are used only to differentiate the individual satellites.

for the observation simulation. Instead, we sub-sample to mimic the effect of the 3x3 averaging, and only take the effect of averaging into account when specifying the effective noise of the resulting observations (see section 4.3). That is, we select every third scan position on every third scanline (with an exception near nadir) i.e. we only use scan positions at 2, 5, 8…50, 53, 57, 60… 108, 111, 114. This method of selection rather than averaging contributes to simulating spatial representation errors, originating from differences in the spatial scales that are represented in the observations and the model fields, and it was found to perform well in previous work.

Spatial/temporal thinning is also applied prior to assimilation which is used for real MW data to mitigate against the presence of spatially correlated errors that are not accounted for in the observation error. These spatially correlated errors primarily arise from representation errors which can also include, for example, radiative transfer errors. Following similar strategies to existing MW instruments, prior to being ingested into the IFS, all the satellites in the EPS-Sterna constellation are thinned together and the same parameters are used for all frequencies. The data are first divided into 30 minute time slots and then spatial thinning is applied where only the observation closest to a T_L255 reduced Gaussian grid point is chosen. The result of the coverage of the data for one 30-minute time slot after this step (combined with the earlier 3x3 selection process) is illustrated for the nominally operational, six-satellite scenario in figure 2. Finally, within the IFS, alternate grid points are selected in the meridional direction. This all culminates in a minimum separation distance of around 110km within each half-hour interval. The phasing of the satellites within each EPS-Sterna constellation is optimised with achieving global coverage as quickly as possible but also to simultaneously minimise the overlap of satellite coverage. This fits well with the thinning strategy applied here where a higher proportion of data will be lost when different satellite coverage overlaps within the 30-minute thinning windows. Figure 2 also provides a snapshot of typical spatial coverage in the 30 minutes that arise from these optimisation criteria.

4.3 Adding noise to EPS-Sterna simulated BTs

Perturbations based on the sample NEDT (as detailed in table 3) divided by three (due to mimicking a 3x3 averaging step) are added to the EPS-Sterna simulated observation prior to assimilation. This step

simulates the instrument noise, assuming no correlation between different samples. For each observation, a random number is drawn from a Gaussian distribution with mean of zero and standard deviation of one. This is multiplied by sample NEDT/3 of the associated channel to give the final perturbation. For the two experiments exploring the impact of changing the NEDT values, the corresponding inflated or reduced values are used in place of the original estimates (table 4). Sensitivity tests performed during the ESA study showed that in fact these perturbations have little impact on the eventual EDA spread changes. The perturbations applied within the EDA, based on the observation error assigned during the assimilation, are larger than the NEDT values and appear to be the dominant factor over these initial perturbations in affecting the spread of the EDA.

4.4 Observation error

The observation error assigned to the EPS-Sterna data during the assimilation follows the established all-sky error model, where the assigned observation error increases in the presence of cloudy signals in either the observations or the model. The all-sky error model has been successfully used for many years at ECMWF and continues to be employed for the latest MW instruments (Geer et al., 2010, 2017). In all-sky use, representation error dominates the observation error in cloudy conditions, arising from different representativeness of clouds in the observations and model fields. To address this, a suitable indicator of the presence of cloud is chosen in order to assign larger errors in situations where a greater amount of cloud is detected in either the observations or model fields (Geer and Bauer, 2011). Inter-channel and spatial error correlations are not explicitly accounted for. While the spatial thinning discussed earlier helps to mitigate against this, the assumed observation errors are also slightly inflated (similar to treatment of e.g. AMSU-A and MHS).

Temperature sounding channels on existing MW instruments use cloud indicators that are constructed with use of lower frequency channels that are unavailable on the EPS-Sterna instrument. Over land a scattering index (23.8-89 GHz) exploits differences in scattering properties of frozen hydrometeors (Bennartz et al., 2002) while over ocean the liquid water path is derived from a combination of 23.8 and 31.4 GHz (Grody et al., 2001). By estimating the cloudy signals in either the observations or model, these indicators control the rate at which the observation error increases from a minimum clear-sky value up to a maximum saturated cloudy value. For existing MW data, these minimum and maximum observation error values are tuned empirically for each frequency and for each satellite. The strategy for defining the key parameters of an adapted version of the observation error model particular for the EPS-Sterna instrument follows the method developed in the ESA small satellite study (further details in Lean et al. (2021b, 2022b)). The maximum assigned observation error in cloudy regions is the same as used for existing real data, as these are dominated by representation error which is expected to be comparable for the EPS-Sterna observations. The observation error assigned in clear-sky regions instead reflects the sample NEDT in combination with smaller representation error contributions. To assign clear-sky observation errors as a function of NEDT we used the same empirical formula as in Lean et al. (2022b), derived from NEDT estimates and assigned observation errors for real data. The cloud indicator adopted for temperature sounding channels on the EPS-Sterna instrument is based on an estimate of the cloud effect in the 52.8 GHz channel, both in the observations and the model background, estimated from comparisons with clear-sky simulations. The same 52.8 GHz indicator is used over both ocean and land surfaces. This has previously been found to be an adequate replacement for the cloud indicators using the lower frequency channels (23.8 and 31.4 GHz) for the AMSU-A or ATMS instrument (Lean et al., 2021b). Note that for the humidity sounding channels, the same cloud indicator used for real MW observations is also applied to the EPS-Sterna instrument where 89 and 165.5 GHz are used to construct a scattering index (Geer et al., 2014).

For the additional sensitivity experiments with inflated or reduced NEDT values, the same empirical formula is applied to obtain the minimum clear-sky observation errors. New maximum errors, $cloudy_{new}$, are also correspondingly increased or reduced by the following equation:

$$cloudy_{new} = \sqrt{cloudy_{orig}^2 - clearsky_{orig}^2 + clearsky_{new}^2} \quad (2)$$

Where the $cloudy_{orig}$ is the original maximum value derived using the unchanged NEDT estimates and $clearsky_{orig}$ and $clearsky_{new}$ are the original and new clear-sky observation errors respectively. In practice, the observation errors of the temperature sounding channels are most affected due to the large component from the NEDT levels. Meanwhile for the humidity sounding channels where minimum clear sky errors are significantly larger than the NEDT due to the more dominant representation error, observation error values are essentially unchanged despite the 30% increase in NEDT.

An important characteristic of the all-sky framework is that the standard deviation of the observation – model background (short-range forecast generated by the previous model cycle) should increase in the presence of cloud in the observations or model, as estimated by the appropriate cloud indicators. The earlier ESA study showed that the simulated data were able to replicate this behaviour. Further checks on the simulated EPS-Sterna data re-confirmed the pattern in the departure statistics including for the new 53.246 GHz channel not previously assimilated at ECMWF (not shown). Note that for later experimentation using the 325 GHz channel set, construction of the observation error will be revisited in the second task of this project. An appropriate model for assimilation of the 325 GHz channels will need to be developed but there will also be consideration as to whether these new channels can improve on the existing cloud indicators for the 183 GHz e.g. as suggested in Eriksson et al. (2020).

4.5 Assimilation

Once the simulated BTs have been thinned and perturbed, they can be assimilated in the EDA experiments where the EPS-Sterna instrument channels follow the same processing as equivalent channels on existing MW instruments. Screening and quality control choices follow the example of real MW data with the exception of channel 3 at 53.246 GHz which has not been used before at ECMWF. This falls between the equivalent of AMSU-A 4 and 5 which have different screening choices due to increased surface sensitivity at the slightly lower frequency. As the instrument channel selection is greatly motivated by the MWS instrument (MWS Science Advisory Group, 2019; EUMETSAT, 2019) this new channel has also been adopted for EPS-Sterna. It is desirable to exploit this new information from the EPS-Sterna instrument but given that there is less experience with real data specifically at this frequency, we take a more cautious approach with limiting the assimilation of the channel to ocean surfaces in the tropical and mid-latitudes. In the future, investigation with real data e.g. from the recently launched MicroWave Temperature Sounder – 3 (MWTS-3) on the Feng-Yun-3E satellite or the future EPS-SG MWS may lead to a more aggressive approach. Some of the key quality control and processing choices are listed in table 5 while more complete details of the all-sky treatment of temperature and humidity sounding instruments in assimilation can be found in Duncan et al. (2022) and Geer et al. (2022) respectively.

During the simulation process, there is no specific addition of systematic errors arising, for example, from errors in the calibration. Nevertheless, the variational bias correction (VarBC) scheme (Auligné et al., 2007) is activated during the assimilation in order that the assimilation system does not treat the EPS-Sterna data as anchor observations i.e. that it would inform the bias correction of other observations. A separate bias correction is applied to each channel on the EPS-Sterna instrument, consistent with the treatment of real MW data. Corrections were confirmed in the earlier ESA study to be small and stable for

Table 5: Summary of key quality control and processing choices made in the assimilation of MW radiances on both the EPS-Sterna instrument and existing MW sounders

Assimilation choice	Application to all-sky MW
Radiative transfer model	RTTOV-SCATT v13 (Saunders et al., 2020; Geer, 2021)
Ocean emissivity	FASTEM-6 (Kazumori and English, 2015)
Land/sea ice emissivity	Dynamic retrieval using 50.3GHz for temperature sounding, 165.5GHz for humidity sounding (Karbou et al., 2006; Baordo and Geer, 2016)
Tropics (<30° N/S) orography rejection	53.246 and 53.596 GHz height < 1000m, 54.4GHz height < 2000m
Extratropics orography rejection	53.246 and 53.596 GHz height < 500m, 54.4GHz height < 1500m
Polar regions (>60° N/S)	53.246, 183±7 and 183±4.5 GHz rejected over all surfaces, 53.596 GHz rejected over land/sea ice in Antarctic region only
Coast	53.246, 53.596, 54.4, 183±7 and 183±4.5 GHz rejected
Snow/sea-ice	53.246, 183±7 and 183±4.5 GHz rejected
Surface sensitive channel rejection	50.3, 52.8, 89, 165.5 GHz not directly assimilated (but used e.g. in emissivity and observation error calculation)

the simulated small satellite data, as required. The approach taken to bias modelling is justified provided biases in the EPS-Sterna data are in line with those experienced in existing MW sounding observations. Observations from high-specification instruments such as those on the Metop or JPSS series of satellites may be necessary to achieve this, for instance, through inter-calibration exercises or other enhanced instrument characterisation.

5 EDA spread results of initial constellations

We begin by discussing some of the key outcomes from analysis of the EDA spread changes which are summarised in figure 3, showing results from EDA experiments with different numbers of real MW sounders as well as the simulated EPS-Sterna scenarios. The respective reduction in EDA spread for each experiment is plotted against the number of assimilated MW sounding locations - this is a total representing the number of locations where one or more channels were used in the assimilation. Geopotential height in the extra-tropics at 500 hPa is shown here as it is a key performance indicator in forecast impact assessment. While all the results are relative to an experiment without MW sounding observations, the reference Baseline to which all the simulated or real data are added/removed is marked with a dotted line (R1 and R2 respectively as detailed in table 1). Figure 3 illustrates the following features which are more generally representative of other variables and pressures:

- All four initial EPS-Sterna constellations result in relatively large spread reductions compared to the Baseline, indicating significant additional benefit. The impact is largest for the constellation with the largest number of satellites (OP4-8SAT) and spread reduction for the four-satellite degraded scenario is larger than the three-satellite scenario. The nominally operational, OP3-6SAT scenario is able to achieve an EDA spread reduction relative to the Baseline that is able to repli-

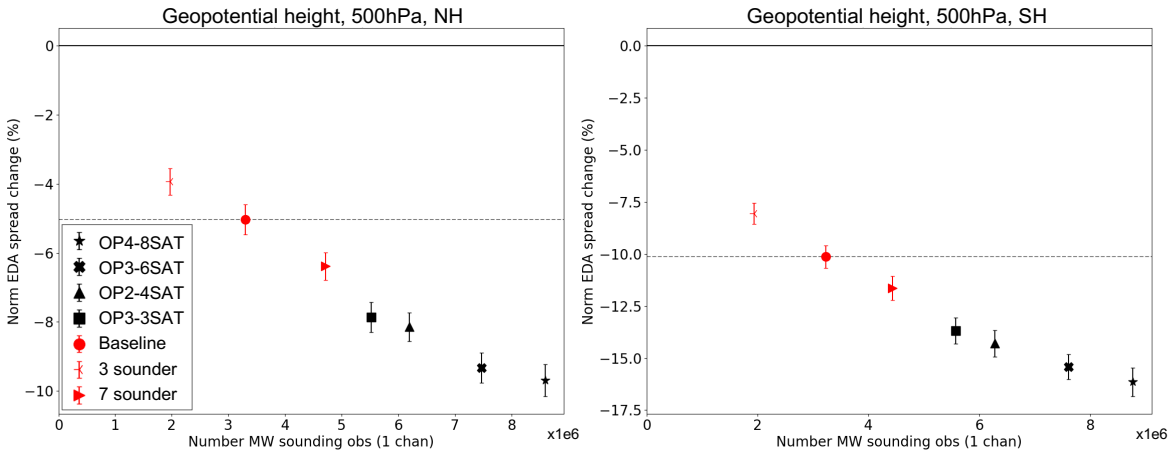

Figure 3: Percentage EDA spread reductions with increasing observation numbers for geopotential height at 500 hPa relative to a No MW Sounding experiment for all EPS-Sterna constellation options and experiments changing the number of MW sounding instruments (R2-R4, table 1). The x-axis denotes the number of observation locations for which one or more channels are assimilated. Different symbols denote the different simulated data scenarios (black) or the use of real MW data (red). The point picked out on the dotted grey line, corresponds to the Baseline to which all other combinations of real and simulated data are added/removed. Data are from the northern hemisphere (latitude $> 20°$N, left panel) and southern hemisphere (latitude $> 20°$S, right panel) over the period 8-28 July 2019. Error bars indicate an estimate of 95% confidence.

cate a large proportion of the positive impact of the Baseline compared to the No MW Sounding experiment.

- At these smaller constellation sizes, as the number of satellites rises the rate of increase in spread reduction remains relatively high. This means the OP3-6SAT constellation achieves an impact that is overall just under twice as large as the OP3-3SAT constellation. Assessment of larger constellations have found that this rate slows more noticeably e.g. for 14-20 small satellites (Lean et al., 2022b).
- A smooth extension in the pattern from experiments changing real data (red points) to addition of simulated data (black points) lends further confidence to the results for the simulated data.

The difference in the magnitude of spread reduction between the northern and southern hemispheres is also demonstrated in figure 3, showing an overall larger impact over the southern hemisphere. This amplification of similar patterns in the southern hemisphere is commonly seen for changes in satellite data as measured by OSEs and is mainly attributed to poorer coverage of conventional observations in this area.

The addition of the simulated EPS-Sterna constellations is also able to produce significant benefit to wind fields as shown in the examples for the U component of wind at 200 hPa (figure 4, upper panels). The inference of wind from adding real MW sounding observations related to temperature and humidity is an important mechanism. There are two key processes in which these impacts on the wind can be indirectly acquired. The first is known as the "4D-Var tracing effect" where the assimilation scheme adds wind increments in response to the temporal evolution of humidity fields. Information from humidity sounding

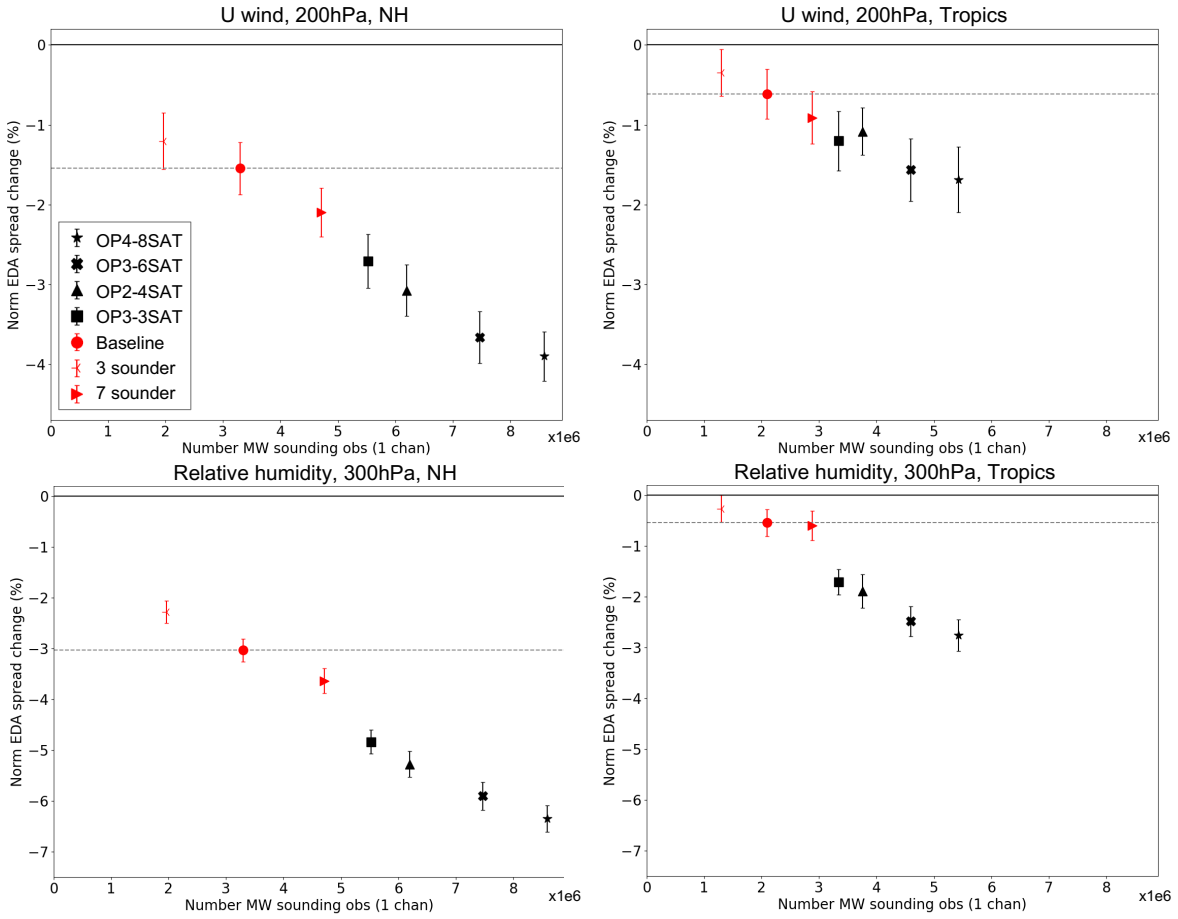

Figure 4: As for figure 3 but for U component of wind at 200 hPa (top row) and humidity at 300 hPa (bottom row) in the northern hemisphere region (latitude $> 20°$N, left column) and tropics region (latitude $\pm$ 20°N, right column).

channels is therefore most influential in the process and effects are predominantly in the troposphere. In the second mechanism, balance equations (e.g. geostrophic balance) link modifications in the mass fields (particularly from temperature sounding observations) to changes in the wind field. The balance relationship is weaker towards the tropics so the 4D-Var tracing effect becomes dominant and humidity sounding channels provide the majority of the benefit for the tropospheric wind at the lower latitudes, whereas in extratropical regions, there is significant additional benefit from the temperature sounding observations on the wind. It is encouraging to see the simulated EPS-Sterna data are also able to similarly affect the wind fields (consistent with previous findings (Lean et al., 2022b)) and the combination of both 50 and 183 GHz results in good impact at all latitudes. Impacts on the U wind in the tropics are generally smaller than the extra-tropics which may be in part due to the strength of the different mechanisms to affect the wind fields, where e.g. the contribution from balance equations lessens in the tropics. However, differences in the magnitude of spread reduction between the tropics and extra-tropics are also seen more widely such as in the examples of relative humidity at 300 hPa (figure 4, lower panels) and can also be linked to fewer data in the tropics. It is important to note that error growth in the tropics is very different to that of the extra-tropics and impacts can be less reliable due to sensitivity to changes in the mean errors.

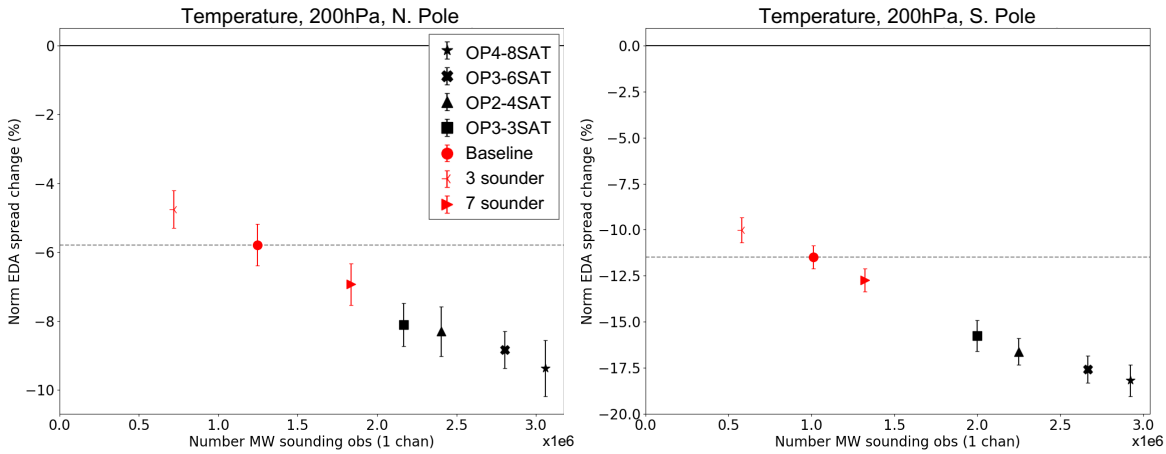

Figure 5: As for figure 3 but for temperature at 200 hPa in the northern polar region (latitude $> 60°$N, left panel) and southern polar region (latitude $> 60°$S, right panel).

In addition to the benefits on hemispheric scales, figure 5 illustrates the similar patterns of significant benefit for temperature at 200 hPa in the polar regions. As for the broader northern/southern hemisphere regions, the spread reduction in the south polar region is much larger than in the north polar region. The geographical variability of the EDA spread values for the nominally operational, six-satellite scenario compared to the Baseline is explored further in examples for the geopotential height at 500 hPa, U wind at 200 hPa and temperature at 850 hPa in figure 6. Here, the dominant blue colour indicates the widespread reduction in EDA spread when adding the EPS-Sterna observations. The dark blue shading confirms larger spread reductions are more concentrated in the polar regions and in particular the southern hemisphere/Antarctica. Meanwhile, the tropics show an overall smaller reduction, consistent with the examples discussed in figure 4. The example of temperature at 850 hPa also illustrates that in the lower troposphere, there is no visible contrast between the improvements over land or ocean surfaces.

As results have so far focused on selected pressure levels, figure 7 gives representative examples of significant reduction in EDA spread for the EPS-Sterna constellations (coloured lines) across the whole vertical profile. Here, the zero line marks the reference Baseline of real observations (R2, table 1) and for comparison the increase in spread (degradation) from the denial of all the MW sounding data (black line) is also included. Across the variables analysed here, the nominally operational OP3-6SAT scenario generally shows spread reductions across all pressures that are around 1.5-1.7 times that of the smallest OP3-3SAT constellation when compared to the Baseline. For a doubling in the number of satellites, a corresponding doubling in the impact would not be expected as previous studies have shown a slowing in the rate of benefit increase (e.g. with addition of real MW data in OSEs (Duncan et al., 2021) and experience with simulating larger small satellite constellations (Lean et al., 2022b)). As the number of satellites differ in each scenario, it is not possible to conclude on the importance of additional orbital planes compared to adding more satellites.

Despite the EPS-Sterna instrument's limited stratospheric sounding capabilities, figure 7 also shows that the benefit from adding EPS-Sterna extends into the stratosphere. Sensitivity from the highest peaking channel (with a broad weighting function peaking around 80 hPa) can contribute to the stratospheric impact and the cycling assimilation scheme is able to propagate changes from the troposphere to these lower pressures. The profiles of the impact on U wind (figure 7, right column) show the smaller impacts

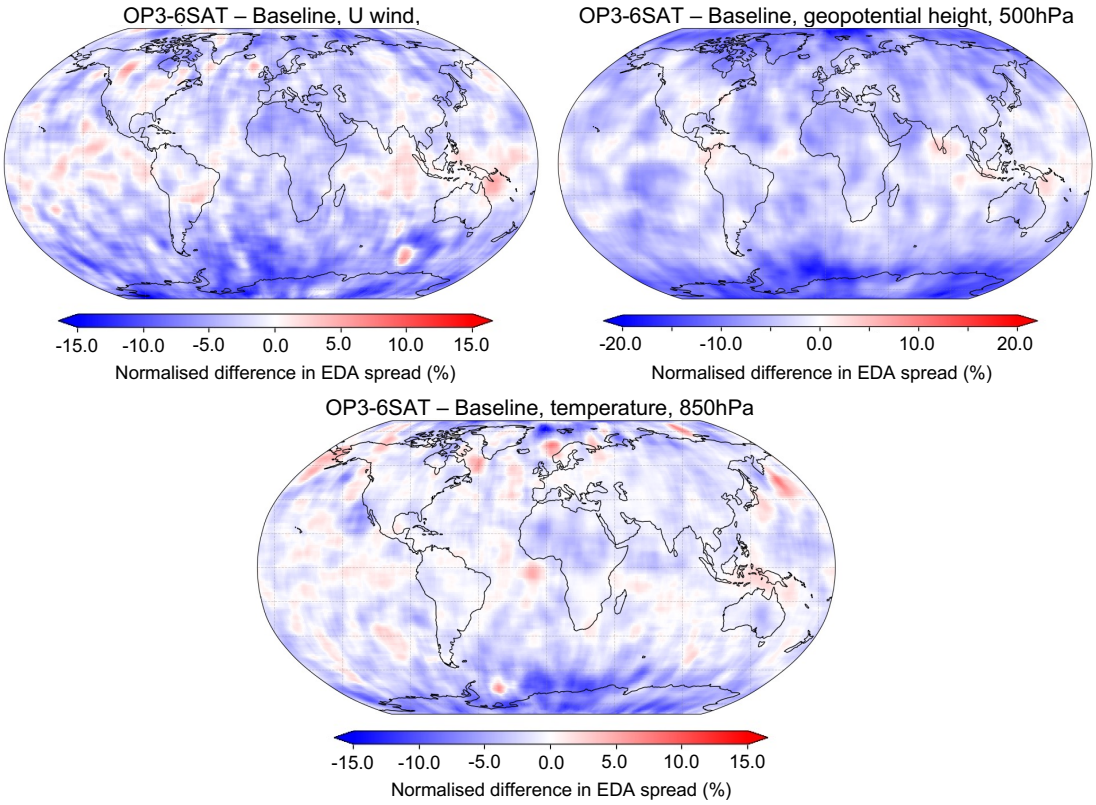

Figure 6: Maps showing the percentage difference in EDA spread between the nominally operational OP3-6SAT EPS-Sterna constellation and the Baseline for U component of wind at 200 hPa (top left panel), geopotential height at 500 hPa (top right panel) and temperature at 850 hPa (bottom panel). Blue colours indicate areas where EDA spread values are smaller in the OP3-6SAT scenario indicating benefit from the addition of the simulated data.

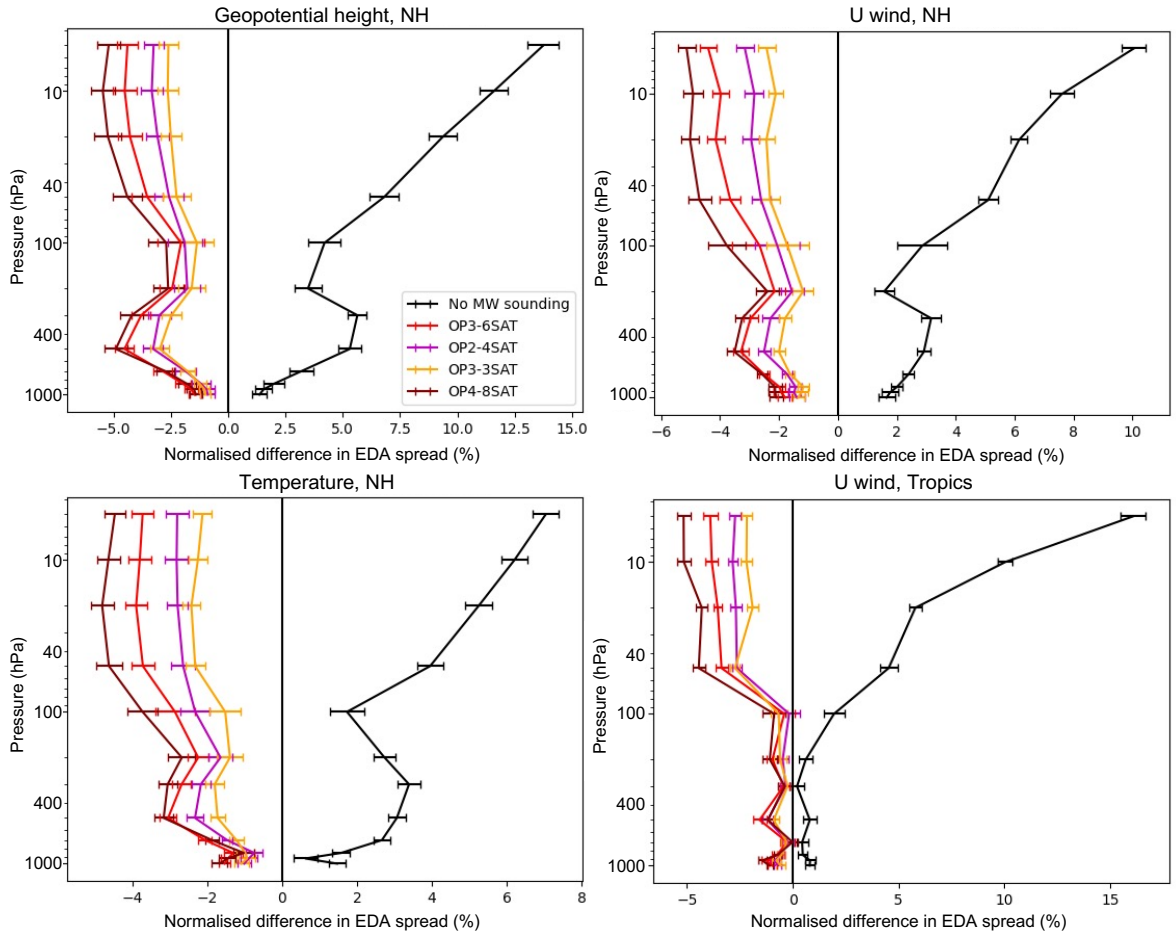

Figure 7: Vertical profiles of EDA spread reduction for (clockwise from top left): geopotential height and U wind in the northern hemisphere (latitude $> 20°$N, left panel), U wind in the tropics (latitude $\pm$ 20°N) and temperature in the northern hemisphere for the EPS-Sterna scenarios and No MW Sounding experiment relative to the Baseline. Data are for the period 8-28 July 2019 and error bars indicate an estimate of 95% confidence.

throughout the troposphere in the tropics (with wind information acquired indirectly mainly from the 4D-Var tracing effect) compared to the extra-tropics (a combination of the 4D-Var tracing effect and balance equations). It is evident that the magnitude of the spread reduction is more comparable between the tropics and extra-tropics in the stratosphere – this is also observed in temperature and geopotential height and is a feature in the real MW observations. However, the troposphere and stratosphere have very different error growth characteristics so the significance of this result is not fully clear.

5.1 Impact of EPS-Sterna relative to changing real observations

We will now further compare the spread reductions from the EPS-Sterna constellations with impact seen from real data, including that of the Metop satellites. Results discussed so far have already provided some evidence that there is significant impact from the four EPS-Sterna constellations when compared with changes to the existing MW sounding constellation. Figure 8 examines this aspect further, showing

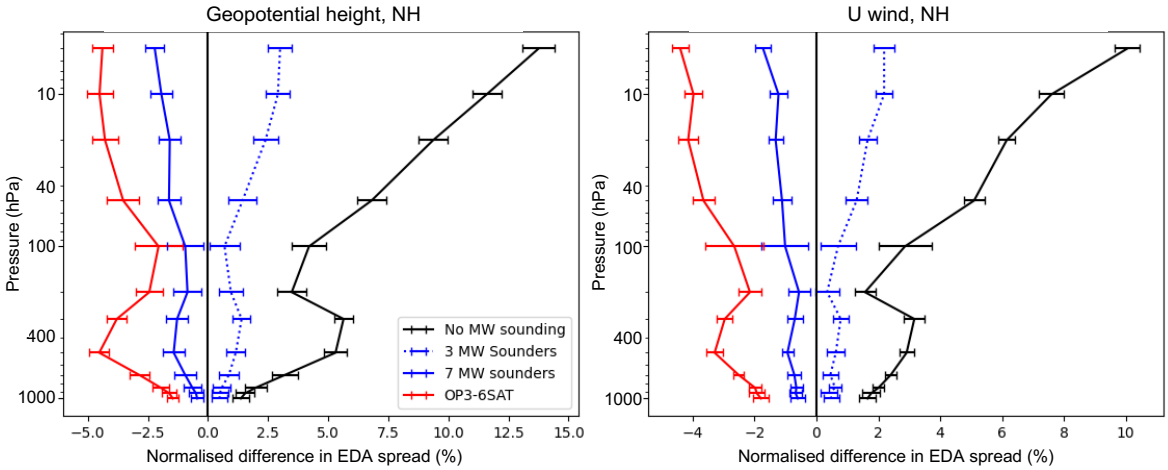

Figure 8: Vertical profiles of EDA spread reduction for the geopotential height (right panel) and U wind (left panel) in the northern hemisphere (latitude $> 20°$N) for the nominally operational OP3-6SAT EPS-Sterna constellation (red) and experiments that change the number of real MW sounding observations (7 MW sounder: solid blue line, 3 MW sounder: dotted blue line) relative to the Baseline (R2). Data are for the period 8-28 July 2019 and error bars indicate an estimate of 95% confidence.

representative examples of the vertical profiles of EDA spread changes for the nominally operational OP3-6SAT EPS-Sterna scenario and experiments concerning changes to the existing MW constellation against the reference Baseline. The OP3-6SAT constellation shows a clear additional reduction in EDA spread compared to the addition of two real polar orbiting MW sounding AMSU-A/MHS pairs ("7 MW sounder ", solid blue line). The removal of two real pairs ("3 MW sounder ", dashed blue line) tends to have a larger spread reduction than the opposite gain when adding a further two pairs (solid blue line). This decrease in the rate of additional impact is a known feature as discussed earlier for the differences in the EPS-Sterna constellations.

Figure 9 compares the OP3-6SAT constellation to the denial of the entire Metop-C platform (solid blue line) and Metop-B/C combined (dashed blue line). The denial of all the MW sounders (black line) is also given for reference. Here, the addition of the OP3-6SAT scenario typically reduces the EDA spread further than the opposite increase in spread from denying Metop-C (but keeping Metop-B). Meanwhile, the loss of both Metop-B/-C shows a larger magnitude of spread change. This suggests that, on these hemispheric scales and with the set of variables considered here, the OP3-6SAT EPS-Sterna constellation would be expected to exceed the impact of a single Metop platform, though would be smaller than that of two Metop platforms. However, it is important to note that the consequences of the loss of a high-performance, multi-sensor platform are not fully captured in the analysis here. For example, our experimentation assumes that high-performance platforms are available for cross-calibration, an aspect that is not captured in the Metop denials shown. In addition, there are benefits from Metop for geophysical variables not considered here, such as atmospheric chemistry or near-surface winds. Near surface wind fields are usually little influenced by changes in MW sounding observations but are affected by measurements from scatterometer instruments. These can be very important in high impact but relatively small spatial scale events such as hurricanes.

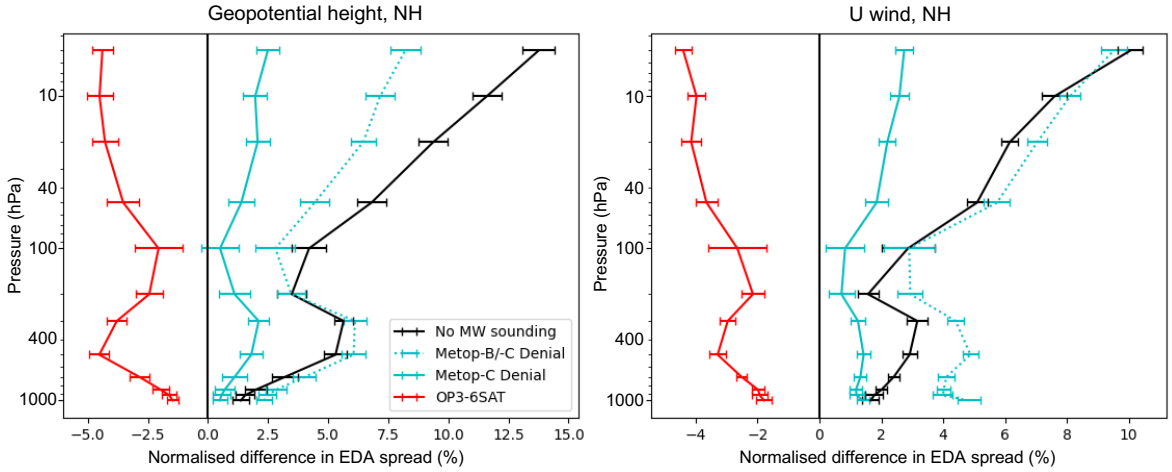

Figure 9: As for figure 8 but comparing the nominally operational OP3-6SAT EPS-Sterna constellation (red line), removal of all MW sounding data (black line) and experiments that change the number of Metop platforms (Metop-C denial: solid blue line, Metop-B/-C denial: dotted blue line) relative to the Baseline (R2).

5.2 Sensitivity to instrument noise performance

Figure 10 shows representative examples of EDA spread changes in the extra-tropics where increasing or reducing the NEDT (and consequently changing the observation errors), can be equivalent to the impact of losing or gaining small satellite platforms respectively in the constellation. By inflating the NEDT consistently by 30%, the spread reduction is between the impact of the original OP3-6SAT and the four-satellite (OP2-4SAT) constellation (red and magenta lines respectively in figure 10). In the southern hemisphere in particular, the result of inflation of the NEDT is closer to the loss of two EPS-Sterna platforms. Conversely, when the temperature sounding NEDT is reduced by around 60%, the additional reduction in EDA spread generally exceeds the benefit of adding two further EPS-Sterna platforms (OP4-8SAT). As only the temperature sounding channels are affected in this case, it highlights the importance of continuing to advocate for excellent noise performance at these frequencies.

In the tropics, where EDA spread impacts are also overall smaller, the change in NEDT does not show a clear improvement or degradation over the original values. Maps of the EDA spread change relative to the original OP3-6SAT experiment (figure 11) show that while the extra-tropics have consistent differences, the tropics are noisier and mixed. The temperature sounding channels are predominantly affected in these experiments and this mass information is more associated with determining larger scale, slower evolving patterns. The ability to capture the finer, faster scale features of the tropics may be less sensitive to changes in the temperature error that still retain relatively small absolute values.

5.3 Combined impact of EPS-Sterna and DWL follow on

The focus in this report has been on assessing EPS-Sterna while a separate study has considered the potential impacts from a DWL follow on mission based on EPS-Aeolus (Healy et al., 2023). Details on the simulation of Aeolus2 data and the assumed observation characteristics can be found in (Healy et al.,

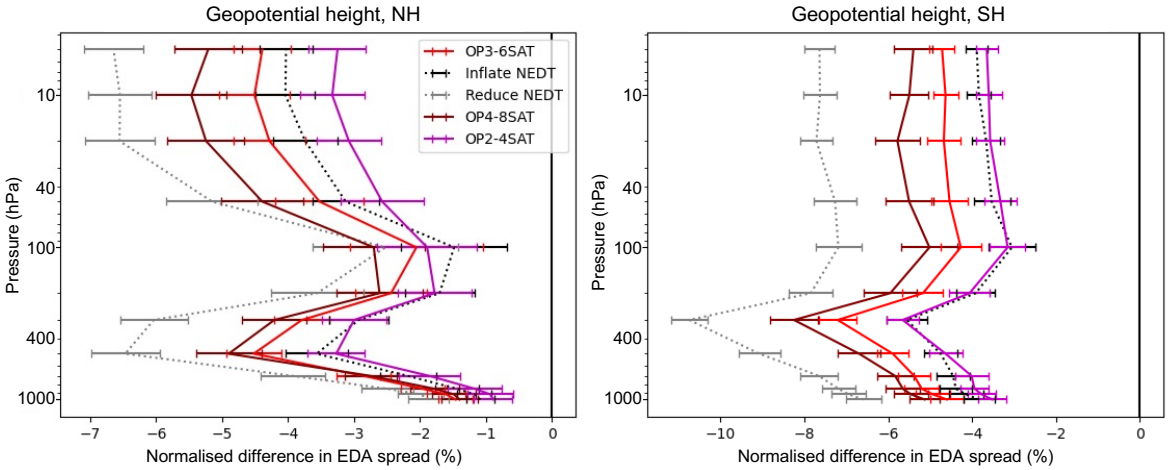

Figure 10: As for figure 8 but for geopotential height in the northern hemisphere (left panel) and southern hemisphere (right panel) comparing the nominally operational six-satellite (OP3-6SAT), degraded four (OP2-4SAT) and enhanced eight-satellite (OP4-8SAT) EPS-Sterna constellations and two experiments that change the noise performance for the six-satellite configuration (inflating NEDT: dotted line, reducing NEDT: dotted blue line) relative to the Baseline (R2).

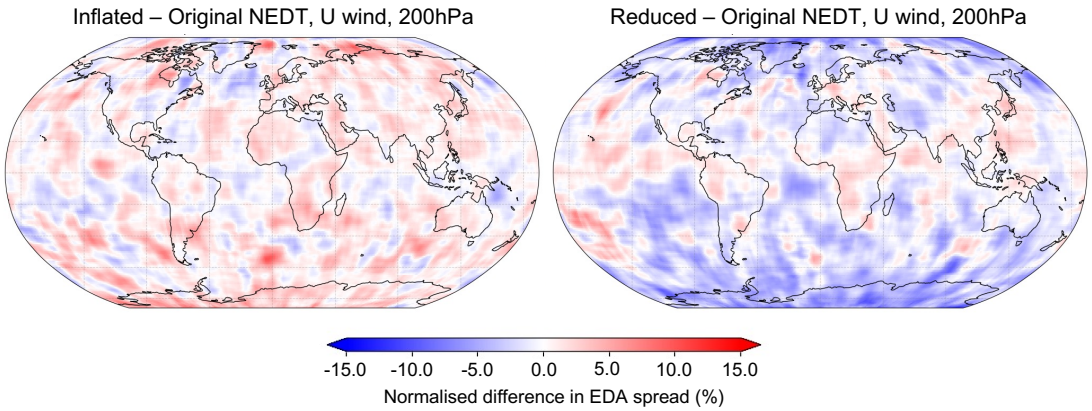

Figure 11: Maps showing the percentage difference in EDA spread between OP3-6SAT using inflated (left) and reduced (right) NEDT values compared to the originally provided values for the U component of wind at 200 hPa. Blue colours indicate areas where the EDA spread values are smaller when using the inflated or reduced NEDT indicating benefit compared to the original NEDT/error values.

2023). Here, we consider the complementarity of the two missions by running a further EDA experiment where both are assimilated. The simulated DWL follow on, "Aeolus2", retains the spatial/temporal and vertical sampling from the current Aeolus mission, but takes into account the better noise performance expected as a result of instrument enhancements over Aeolus. Figure 12 shows that when both missions are included, there is a significant further spread reduction beyond the individual contributions and the overall impact retains a high proportion of the separate spread reductions if they were simply added. Figure 12 highlights the different strengths of Aeolus2 and EPS-Sterna that make the missions complementary in their impacts. For example, the impact on tropospheric tropical winds is much higher for Aeolus2 and forms the dominant component of the combined impact while for geopotential height and temperature, a higher contribution to the combined impact comes from EPS-Sterna, particularly over the extra-topics. The spread reductions of both individual missions compare favourably to the magnitude of the opposite spread increase from denying Metop-C across all the variables considered. The combined impact is far greater in the measures used here than the removal of a single multi-sensor platform.

Using the example of the U component of wind at 500 hPa, figure 13 further shows the complementary impacts of Aeolus2 and EPS-Sterna that result in significantly reducing the EDA spread globally. Supporting the trends seen in figure 12, Aeolus2 has higher impact in the tropics while in the extra-tropics, the spread reductions are similar in magnitude to EPS-Sterna. However, the widespread darker blue colours that indicate significant benefit from the combined experiment reinforces the additive nature of the impacts and the resulting global improvements. Provided the missions perform as expected, this is likely a lower estimate of the combined benefit of EPS-Sterna and EPS-Aeolus, as only the noise performance has been accounted for in the simulated Aeolus2 and the 325 GHz channels on EPS-Sterna have not been added.

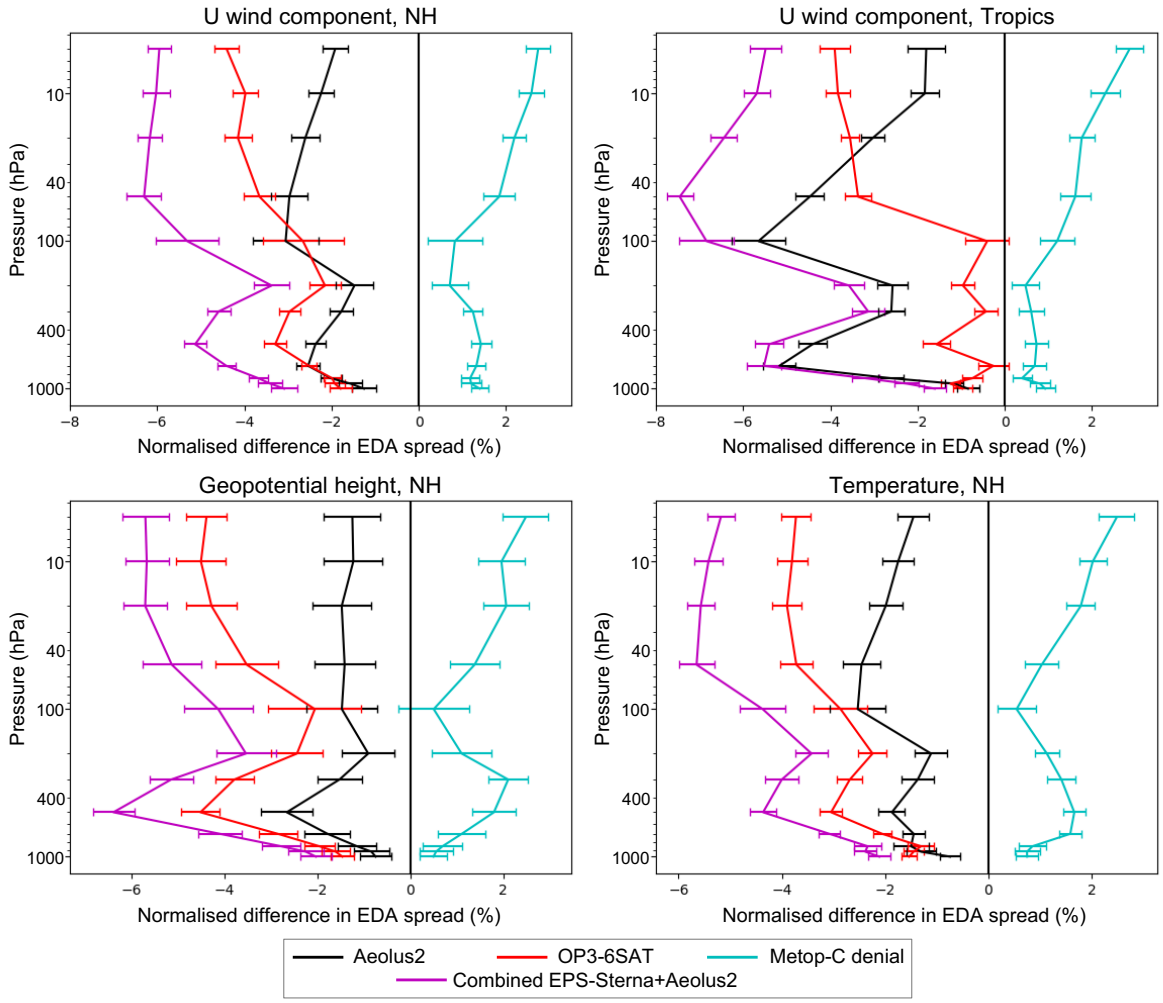

Figure 12: Vertical profiles of EDA spread reduction for (clockwise from top left): U wind in the northern hemisphere (latitude $> 20°$N) and in the tropics (latitude $\pm$ 20°N), temperature and geopotential height in the northern hemisphere for the nominally operational six-satellite EPS-Sterna scenario, Aeolus2 and the combination of both missions in a further EDA experiment relative to the Baseline. For comparison, the denial of all data used on Metop-C is also shown. Data are for the period 8-28 July 2019 and error bars indicate an estimate of 95% confidence.

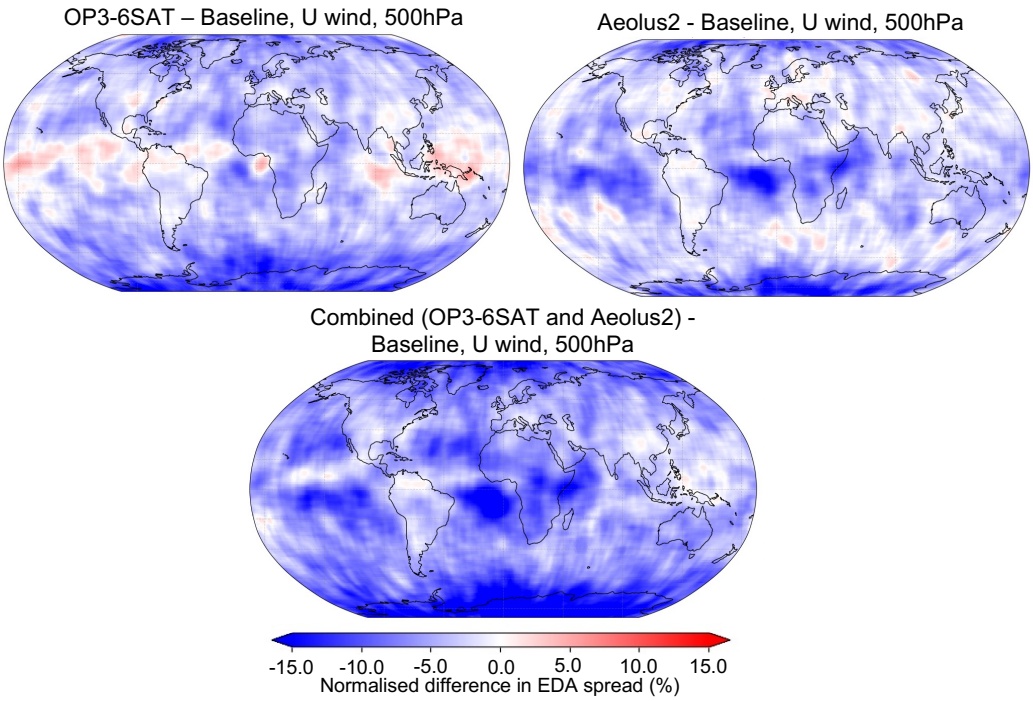

Figure 13: Maps showing the percentage difference in EDA spread between the nominally operational EPS-Sterna constellation, OP3-6SAT (top left), Aeolus2 (top right) and the combination of both in a further EDA experiment (bottom panel) compared to the Baseline for the U component of wind at 500 hPa. Blue colours indicate areas where the EDA spread values are smaller when adding separately or together the EPS-Sterna and Aeolus2 missions indicating benefit compared to the Baseline.

6 Summary and next steps

This report first reviews the EDA technique and outlines the steps to simulate and assimilate EPS-Sterna observations along with their accompanying observation errors. We then present the evaluation of the benefit to global NWP from a set of initial EPS-Sterna constellations (focusing on 50 and 183 GHz sounding channels alongside two window channels). An earlier ESA study which employed the EDA method to assess future constellations of small satellites carrying MW sounders (Lean et al., 2022b) provided a framework that is adapted here to different configurations for EPS-Sterna. In the EDA approach, reductions in EDA spread indicate reductions in the forecast uncertainties and therefore a benefit to NWP. The key steps to simulating and assimilating the EPS-Sterna observations have been outlined, including highlighting limitations, such as the need to use simple emissivity estimates over challenging snow/sea-ice surfaces during the simulation. Adaptations for the EPS-Sterna instrument were also discussed such as the formulation of the all-sky observation error model (where observation errors increase in the presence of cloudy signals in either the observations or the model). For temperature sounding channels on existing MW instruments, the cloud indicator, which forms the basis for the rate of increase of the observation error in the presence of cloud signals, uses low frequency channels unavailable on the EPS-Sterna instrument. Therefore, an alternative cloud indicator is employed based on 52.8 GHz that was previously developed and tested for small satellites with similar limitations (Lean et al., 2021b). New parameters have been calculated using a formula derived in earlier work to define the minimum

clear-sky error and the maximum saturated cloudy error.

Four initial potential EPS-Sterna constellation options have so far been tested comprising of the nominal six-satellite scenario (three orbital planes each with two satellites), two "degraded" scenarios, OP3-3SAT (three orbital planes each with one satellite) and OP2-4SAT (two orbital planes each with two satellites) and an "enhanced scenario" (four orbital planes each with two satellites). Additional EDA experiments that investigate impacts from changes to the real observing system (either from changing only the number of existing MW sounding observations or removal of entire Metop platforms) lend context to the magnitude of the benefit seen for EPS-Sterna. All addition of simulated data or addition/denial of real data is made relative to a reference baseline (referred to as the "Baseline") of real observations. In this Baseline, the number of MW sounding instruments is reduced to consist of five polar orbiting temperature and humidity sounding instrument pairs, representing the afternoon, early- and mid-morning orbits, plus GMI. This is chosen to reflect a potential future with fewer large satellite platforms. Key points from the analysis are:

- All four EPS-Sterna constellations show a significant EDA spread reduction with larger impacts as the number of observations increases. The rate of the spread reduction remains relatively high such that the OP3-6SAT scenario reduces the spread on average around 1.5-1.7 times that of the OP3-3SAT scenario when compared to the Baseline system of real observations. The scenario with four satellites in two orbital planes performs better than the scenario with three satellites in three orbital planes.
- Significant benefits are in general observed across the variables, pressures and geographical regions analysed including impact on wind fields arising indirectly as a result of the 4D-Var tracing effect and balance equations. The magnitude of the impact varies across geographical region with largest changes in spread observed in the southern hemisphere and smallest in the tropics (consistent with previous findings (Lean et al., 2022b)).
- The magnitude of the impact of the OP3-6SAT EPS-Sterna scenario relative to the Baseline is able to replicate a large proportion of benefit from the Baseline relative to an experiment denying all the MW sounding observations. OSEs with real MW data suggest that this would translate to significant positive impacts on forecast error statistics (Duncan et al., 2021).
- The EDA spread reduction from the addition of the OP3-6SAT scenario was also shown to be slightly larger in magnitude than the opposite spread increase when removing the entire Metop-C platform (both relative to the Baseline). The removal of both Metop-B and -C resulted in a significantly larger spread increase. While this indicates a strong benefit from the OP3-6SAT EPS-Sterna constellation, the EDA spread reduction metric used here does not fully capture the value of these large multi-sensor Metop platforms. The loss of a large platform will affect many other aspects such as land surface parameters, the role of GNSS-RO in providing "anchor" observations (around 600 radio occultation profiles are used a day from a single Metop platform) that help inform the bias correction of other observations, surface winds and atmospheric composition. Furthermore, a complementary backbone of high-performance satellite platforms also provide essential calibration information for small satellite instruments.

Further sensitivity experiments investigated the impact of the instrument noise performance where the nominally operational six-satellite scenario was rerun firstly with the NEDT for all channels inflated by 30% and secondly with the NEDT for the temperature sounding channels reduced by around 60%. The changes in NEDT (and associated observation errors) results in significant impacts on the EDA spread

reduction. The inflation of NEDT resulted in a smaller spread reduction equivalent in the extra-tropics to the loss of between one and two EPS-Sterna platforms. Meanwhile the reduced NEDT experiment showed additional spread reduction exceeding the impact of adding a further two satellites to the constellation. In the tropics, changes were small suggesting that the noise performance of the temperature sounding channels, within the range tested here, was less important in this region. The performance of EPS-Sterna with the anticipated on-orbit NEDT values is significant however, the overall large differences in impact from small changes in absolute values of NEDT highlight the worth of pursuing ambitious noise performance targets, particularly for temperature sounding channels around the 50 GHz band. The noise performance should be an important consideration for future small satellites where trade-offs in creating smaller platforms may lead to compromises in performance. More generally, this can also motivate design of instruments on large platforms where there may be more opportunity to construct low noise sensors.

After finding significant benefits individually from EPS-Sterna and, in a separate project, a DWL follow on to Aeolus, (Aeolus2, based on the future EPS-Aeolus mission), a further experiment found large additional EDA impacts from combining the two missions. Separately, the two missions have different strengths such as much larger impacts on tropical winds for Aeolus2 but greater benefit in other variables such as geopotential height from EPS-Sterna. The EDA spread reduction for the combined case is quite additive of the individual contributions meaning that globally and across different pressure levels the good complementarity leads to overall significant positive impact above either mission alone. The magnitude of the spread reduction for the combined impact is much greater than the opposite degradation seen when removing a single Metop platform. As the increased spatial/temporal sampling from EPS-Aeolus and 325 GHz channels on EPS-Sterna have not been accounted for here, the impact presented here is also expected to be a conservative estimate of the potential future benefit.

In the next steps of this project, we use the results presented here to inform the design of the constellations still to be tested and establish a benchmark to assess the additional impact of the 325 GHz channels, new to a space-borne platform. Development of techniques to simulate and assimilate the 325 GHz channel is ongoing as part of task 1.2. The final set of potential EPS-Sterna constellations will be evaluated in task 1.3 using the complete set of EPS-Sterna instrument channels.

References

Arnold, C. P., J., Dey, C.H., 1986. Observing-Systems Simulation Experiments: Past, Present, and Future. Bulletin of the American Meteorological Society 67, 687–695. doi:10.1175/1520-0477(1986)067<0687:OSSEPP>2.0.CO;2.

Atkinson, N., 2015. NE△T specification and monitoring for microwave sounders. NWP SAF Technical Report, version 1.1 Doc ID: NWPSAF-MO-TR-033, 12pp.

Auligné, T., McNally, A.P., Dee, D.P., 2007. Adaptive bias correction for satellite data in a numerical weather prediction system. Q.J.R.M.S. 133, 631–642. doi:https://doi.org/10.1002/qj.56.

Baordo, F., Geer, A., 2016. Assimilation of SSMIS humidity-sounding channels in all-sky conditions over land using a dynamic emissivity retrieval. Q.J.R.M.S. , 2854–2866doi:https://doi.org/10.1002/qj.2873.

Bell, W., Di Michele, S., Bauer, P., McNally, T., English, S.J., Atkinson, N., Hilton, F., Charlton, J., 2010. The Radiometric Sensitivity Requirements for Satellite Microwave Temperature Sound-

ing Instruments for Numerical Weather Prediction. J. Atmos. Oceanic Technol. 27, 443–459. doi:https://doi.org/10.1175/2009JTECHA1293.1.

Bell, W., English, S.J., Candy, B., Atkinson, N., Hilton, F., Baker, N., Swadley, S.D., Campbell, W.F., Bormann, N., Kelly, G., Kazumori, M., 2008. The Assimilation of SSMIS Radiances in Numerical Weather Prediction models. IEEE Transactions on Geoscience and Remote Sensing 46, 884–900. doi:10.1109/TGRS.2008.917335.

Bennartz, R., Thoss, A., Dybbroe, A., Michelson, D., 2002. Precipitation analysis using the Advanced Microwave Sounding Unit in support of nowcasting applications. Met. Apps , 177–189doi:https://doi.org/10.1017/S1350482702002037.

Bonavita, M., Isaksen, L., Holm, E., 2012. On the use of EDA background error variances in the ECMWF 4D-Var. Quart. J. Roy. Meteorol. Soc 138, 1540–1559.

Bonavita, M., Raynaud, L., Isaksen, L., 2011. Estimating background-error variances with the ECMWF Ensemble of Data Assimilations system: some effects of ensemble size and day-to-day variability. Quart. J. Roy. Meteorol. Soc. , 423–434.

Bormann, N., Fouilloux, A., Bell, W., 2013. Evaluation and assimilation of atms data in the ecmwf system. Journal of Geophysical Research: Atmospheres , 12,970–12,980doi:https://doi.org/10.1002/2013JD020325.

Bormann, N., Lawrence, H., Farnan, J., 2019. Global observing system experiments in the ECMWF assimilation system. ECMWF Technical Memorandum No.839.

Cardinali, C., Žagar, N., Radnoti, G., Buizza, R., 2014. Representing model error in ensemble data assimilation. ECMWF Technical Memorandum .

Coordination Group for Meteorological Satellites, 2022. CGMS Baseline: Sustained contributions to the observing of the Earth system, space environment and the Sun. Available online at https://cgms-info.org/publication/cgms-baseline/ (Accessed 1 Aug 2022) CGMS/DOC/18/1028862, v.4.

Duncan, D.I., Bormann, N., 2020. On the Addition of Microwave Sounders and NWP Skill, Including Assessment of FY-3D Sounders. EUMETSAT/ECMWF Fellowship Programme Research Report No.55.

Duncan, D.I., Bormann, N., Geer, A.J., Weston, P., 2022. Assimilation of AMSU-A in All-Sky Conditions. Monthly Weather Review 150, 1023 – 1041. doi:10.1175/MWR-D-21-0273.1.

Duncan, D.I., Bormann, N., Hólm, E.V., 2021. On the addition of microwave sounders and numerical weather prediction skill. Q. J. R. Meteorol. Soc. 147, 3703–3718. doi:https://doi.org/10.1002/qj.4149.

Eriksson, P., Kaur, I., Pfreundschuh, S., 2020. Study to support the definition of Arctic Weather Satellite (AWS) high frequency channels. EUMETSAT Contract EUM/CO/20/4600002417/CJA Final Report , 41ppURL: https://research.chalmers.se/en/publication/519309.

EUMETSAT, 2019. Considerations on user requirements for additional mini-Microwave sounders. EUM/STG/75/19/DOC/18 .

Geer, A., Ahlgrimm, M., Bechtold, P., Bonavita, M., Bormann, N., English, S., Fielding, M., Forbes, R., Hogan, R., Hólm, E., Janiskova, M., Lontiz, K., Lopez, P., Matricadi, M., Sandu, I., Weston, P., 2017. Assimilating observations sensitive to cloud and precipitation. ECMWF Technical Memorandum No.815.

Geer, A., Baordo, F., Bormann, N., English, S., 2014. All-sky assimilation of microwave humidity sounders. ECMWF Technical Memorandum No. 741, 57pp.

Geer, A., Bauer, P., Lopez, P., 2010. Direct 4D-Var assimilation of all-sky radiances. Part II: Assessment. ECMWF Technical Memorandum No.619.

Geer, A.J., 2021. Physical characteristics of frozen hydrometeors inferred with parameter estimation. Atmospheric Measurement Techniques 14, 5369–5395. URL: https://amt.copernicus.org/articles/14/5369/2021/, doi:10.5194/amt-14-5369-2021.

Geer, A.J., Bauer, P., 2011. Observation errors in all-sky data assimilation. Q. J. R. Meteorol. Soc. 137, 2024–2037. doi:doi:10.1002/qj.830.

Geer, A.J., Bauer, P., Lonitz, K., Barlakas, V., Eriksson, P., Mendrok, J., A. Doherty, J.H., Chambon, P., 2021. Bulk hydrometeor optical properties for microwave and sub-millimetre radiative transfer in RTTOV-SCATT v13.0. Geosci Model Dev 14, 7497–7526. doi:10.5194/gmd-14-7497-2021.

Geer, A.J., Lonitz, K., Duncan, D., Bormann, N., 2022. Improved surface treatment for all-sky microwave observations. ECMWF Technical Memoranda URL: https://www.ecmwf.int/node/20337, doi:10.21957/zi7q6hau.

Grody, N., Zhao, J., Ferraro, R., Weng, F., , Boers, R., 2001. Determination of precipitable water and cloud liquid water over oceans from the NOAA 15 advanced microwave sounding unit. J. Geophys. Res. , 2943–2953doi:doi:10.1029/2000JD900616.

Hallegatte, S., Eyre, J., McNally, T., Potthast, R., Husband, R., 2014. The case for the eumetsat polar system (eps)/metop second-generation programme: Cost benefit analysis. Yearbook on Space Policy 2011/2012: Space in Times of Financial Crisis, Springer Vienna , 193–213URL: https://doi.org/10.1007/978-3-7091-1649-4_7, doi:10.1007/978-3-7091-1649-4_7.

Harnisch, F., Healy, S.B., Bauer, P., English, S.J., 2013. Scaling of GNSS Radio Occultation Impact with Observation Number Using an Ensemble of Data Assimilations. Mon. Wea. Rev. 141, 4395–4413. doi:doi:http://dx.doi.org/10.1175/MWRD-13-00098.1.

Healy, S.B., Lean, K., Semane, N., Bormann, N., 2023. Task 2: Doppler Wind Lidar EDA Impact Assessment. EUMETSAT Contract EUM/CO/22/4600002673/SDM Final Report, ECMWF, Reading, UK .

Isaksen, L., Bonavita, M., Buizza, R., Fisher, M., Haseler, J., Leutbecher, M., Raynaud, L., 2010. Ensemble of data assimilations at ECMWF. ECMWF Technical Memorandum No.636, pp. 45. URL: https://www.ecmwf.int/node/10125, doi:10.21957/obke4k60.

Karbou, F., Gérard, E., Rabier, F., 2006. Microwave land emissivity and skin temperature for AMSU-A and -B assimilation over land. QJRMS 132, 2333–2355.

Kazumori, M., English, S.J., 2015. Use of the ocean surface wind direction signal in microwave radiance assimilation. QJRMS 141, 1354–1375. URL: https://rmets.onlinelibrary.wiley.com/doi/abs/10.1002/qj.2445, doi:doi:10.1002/qj.2445.

Lagaune, B., Sten, B., Emrich, A., 2021. Arctic Weather Satellite, A microsatellite constellation for improved weather forecasting in Arctic and globally. Proceedings of the AIAA/USU Conference on Small Satellites, Mission Lessons, SSC21-XII-02, Logan, Utah, U.S.A. URL: http://digitalcommons.usu.edu/smallsat/2021/all2021/213/.

Lean, K., Bormann, N., Healy, S., 2021a. Technical Note 1 for ESA Contract No. ESA 4000130590/20/NL/IA: WP-1000 Review of EDA approach and recommendations for small satellite configurations. ESA Contract 4000130590/20/NL/IA Technical Note 1 URL: https://www.ecmwf.int/node/20304, doi:10.21957/osvhislk.

Lean, K., Bormann, N., Healy, S., 2021b. Technical Note 2 for ESA Contract No. ESA 4000130590/20/NL/IA: WP-2000 Calibration of EDA spread and adaptation of the observation error model. ESA Contract 4000130590/20/NL/IA Technical Note 2 URL: https://www.ecmwf.int/node/20302, doi:10.21957/1auh0nztg.

Lean, K., Bormann, N., Healy, S., 2022a. Technical Note 3 for ESA Contract No. ESA 4000130590/20/NL/IA: WP-3000 Developing a flexible system to simulate and assimilate small satellite data. ESA Contract 4000130590/20/NL/IA Technical Note 3 URL: https://www.ecmwf.int/node/20303, doi:10.21957/kjmxyh9xy.

Lean, K., Bormann, N., Healy, S., English, S., 2022b. Final Report for ESA Contract No. ESA 4000130590/20/NL/IA: Final Report: Study to assess earth observation with small satellites and their prospects for future global numerical weather prediction. ESA Contract 4000130590/20/NL/IA Final Report URL: https://www.ecmwf.int/en/elibrary/81324-final-report-study-assess-earth-observation-small-satellites-and-their-prospects, doi:10.21957/kp7z1sn1n.

Lonitz, K., Marquardt, C., Bowler, N., Healy, S., 2021. Final Technical Note of Impact assessment of commercial GNSS-RO data. ESA contract 4000131086/20/NL/FF/a Final Report URL: https://www.ecmwf.int/node/20240, doi:10.21957/wrh6voyyi.

Masutani, M., Andersson, E., Terry, J., Reale, O., Jusem, J., Riishøjgaard, L., Schlatter, T., Stoffelen, A., Woollen, J., Lord, S., Tóth, Z., Song, Y., Kleist, D., Xie, Y., Prive, N., Liu, E., Sun, H., Emmitt, D., Boukabara, S.A., 2007. Progress in joint osses a new nature run and international collaboration. AMS preprint volume for 18th conference on Numerical Weather Prediction, Parkcity, Utah. 25 - 29 June 2007 .

Masutani, M., Schlatter, T., Errico, R., Stoffelen, A., Andersson, E., Lahoz, W., Woollen, J., Emmitt, G., Riishøjgaard, L.P., Lord, S., 2010. Data Assimilation: Making sense of observations, Observing System Simulation Experiments. Eds. W.A. Lahoz, B. Khattatov and R. Ménard, Springer , 647–679.

MWS Science Advisory Group, 2019. EPS-SG MicroWave Sounder (mws) science plan - version 1.0 EUMETSAT EPS-SG Resources, 102pp. URL: https://www.eumetsat.int/media/43204.

Palmer, T., Buizza, R., Doblas-Reyes, F., Jung, T., Leutbecher, M., Shutts, G., Steinheimer, M., Weisheimer, A., 2009. Stochastic parametrization and model uncertainty. ECMWF Technical Memorandum , 42.

Saunders, R., Hocking, J., Turner, E., Havemann, S., Geer, A., Lupu, C., Vidot, J., Chambon, P., Köpken-Watts, C., Scheck, L., Stiller, O., Stumpf, C., Borbas, E., 2020. RTTOV-13 science and validation report. EUMETSAT NWP SAF, version 1.0 URL: https://nwp-saf.eumetsat.int/site/software/rttov/documentation/.

Tan, D.G.H., Andersson, E., Fisher, M., Isaksen, L., 2007. Observing-system impact assessment using a data assimilation ensemble technique: Application to the ADM-Aeolus wind profiling mission. Quart. J. Roy. Meteor. Soc. 133, 381–390.